J. Fluid Mech. (1987), *vol.* 176. *pp.* 135–167
Printed in Great Britain

Interaction of an unstable planar jet with an oscillating leading edge

By THOMAS STAUBLI† AND DONALD ROCKWELL
Department of Mechanical Engineering and Mechanics, Lehigh University, Bethlehem, PA 18015, USA

(Received 3 September 1985 and in revised form 9 June 1986)

An inherently unstable jet impinges upon a leading edge oscillating at controlled frequency and displacement amplitude, giving rise to two coexisting instability waves in the jet: one at the self-excited frequency of the jet; and the other at the controlled frequency of the edge displacement. Correspondingly there is an unsteady loading of the edge at these two frequencies. Simultaneous edge pressure and jet velocity measurements allow insight into the upstream influence, arising from the edge loading, on the jet oscillations. This upstream influence initially distorts the jet at the nozzle exit and causes non-homogeneous phase variations along the streamwise extent of the jet. A simple superposition model which includes upstream-induced velocities and instability-wave velocities effectively simulates these distortions.

The jet oscillations synchronize with the frequency of the controlled edge oscillations for excitation frequencies close to those of the natural jet oscillations. Measurement of the pressure amplitudes on the edge surface shows resonance of the component at the excitation frequency within the synchronization range, and attenuation of the component at the self-excited frequency close to the synchronization range. Depending on the amplitude of edge displacement, synchronization is achieved either by quenching of the self-excited component or by phaselocking of the self-excited component to the excitation frequency. Phase measurements between edge displacement and surface pressure fluctuation allow determination of the direction of energy transfer between the flow and the edge.

Flow-visualization performed simultaneously with pressure measurements gives insight into the relation between impinging vortical structures and pressure fluctuations. Time-sequence photographs allow analysis of the modulation of the flow structure due to coexistence of the self-excited and the externally excited jet instabilities. Vortex coalescence involving vortices of like sense, as well as typical formations of pairs of counter-rotating vortices, are observed. Retardation of the development of the jet vortex pattern occurs when the energy transfer from the flow to the edge is a maximum. At high excitation frequency, the large-scale jet structure recovers to that occurring in absence of edge oscillations.

1. Introduction – flow and feedback mechanisms of the stationary and oscillating leading edge

The basic features of self-sustained oscillations of a jet incident upon an edge were defined over two decades ago in a series of investigations by Powell (1961, 1962, 1965). In essence, the inherently unstable jet impinges upon a stationary edge; the interaction of the incident jet with the edge serves as a source of periodic upstream

† Present address: Sulzer Escher Wyss, Hydraulic Development, CH-8023 Zürich, Switzerland.

influence to the disturbance-sensitive region of the jet at the nozzle lip. In turn, selective amplification in the jet controls the growth of the jet instability downstream of the nozzle. The periodicity of the upstream influence and thereby of the initial excitation in the sensitive region near separation leads to highly organized jet–edge interactions. Much attention has been focused on various details of this class of flows, as assessed by Rockwell (1983). Recent advances have characterized the streamwise evolution of the unstable jet including disturbance growth rates (Lucas & Rockwell 1984), as well as streamwise phase variations (Shields 1967), allowing comparison with linear stability theory. Regarding the impingement of the oscillating jet upon the leading edge, attention has been given to mechanisms of vortex–edge interaction (Lucas & Rockwell 1984) and the consequent unsteady pressure field along the surface of the edge (Kaykayoglu & Rockwell 1986). It is this loading upon the edge by the unsteady pressure field that determines the character and strength of the upstream influence. Since this edge interaction region is central in determining the upstream influence, it follows that controlled perturbations of the edge itself would provide further insight.

Figure 1 shows, with a photograph and a schematic, the principle features of self-sustained oscillations of the jet impinging upon a stationary edge. The figure also induces a control-type representation of the upstream influence. The frequency f_0^* designates the frequency at which a disturbance in the shear layer of the jet undergoes maximum amplification and thereby leads to an instability wave. This instability of the jet initially takes the form of an amplified undulation; at sufficiently high Reynolds number and over long enough steamwise distance, the instability leads to formation of one or more vortices upstream of the edge. The unsteady flow patterns repeat alternatingly and symmetrically on either side of the edge regardless of the character of the jet instability approaching the edge. This jet–edge interaction in turn causes pressure fluctuations on the lower and upper sides of the edge which are π out of phase with respect to each other. The resulting unsteady pressure loading determines the dominant contribution to the upstream-induced disturbances felt at the nozzle exit, i.e. upstream influence. If, as for the case examined in this paper, a typical acoustic wavelength is much larger than the impingement length L, this upstream influence is felt essentially instantaneously throughout the flow domain and the entire process may be viewed as incompressible.

According to the concept advanced by Powell (1961) this upstream influence emanates from the leading-edge region and can be represented by a distribution of dipole sources along the edge. Their strength is directly related to the pressure distribution on the edge surface. In the actual case with jet flow, the jet will be exposed to such a dipole-induced flow field causing a transverse motion of the jet. According to Powell: 'If this motion were uniform along the length of the jet, it could induce no distortion of the jet, simply translating it *en masse*; with the motion attributable to a dipole at the edge, the lateral motion must increase as the edge is approached and this must cause some distortion of the stream. But the greatest and really significant distortion occurs as the jet leaves the nozzle, since the part within is altogether constrained from motion while that without moves with the surrounding fluid'. Thus, the dipole-induced transverse velocity, enhanced in the vicinity of the nozzle exit by the presence of the nozzle, causes the initial perturbation of the jet. For purposes of illustration, figure 2 shows computed streamlines that are obtained by approximating the induced flow field and its distortion by the nozzle with a single dipole at the edge and by applying conformal mapping as suggested by Powell.

In general, the velocity and pressure fluctuations of the jet will contain contribu-

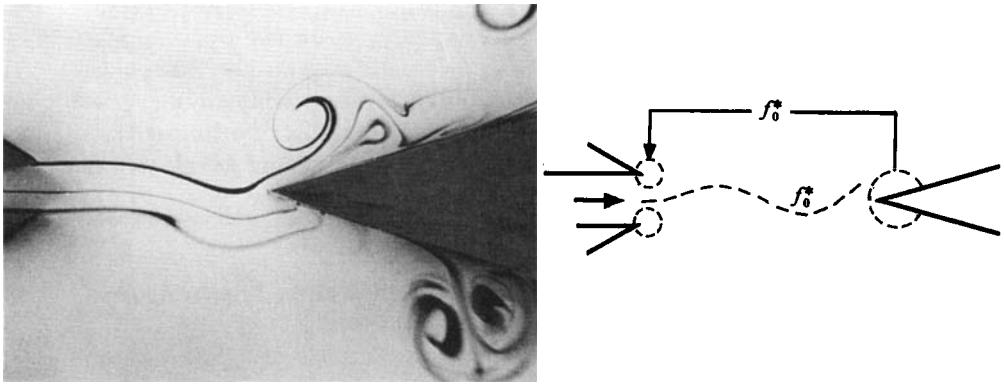

FIGURE 1. Self-sustained oscillations of a jet impinging upon a stationary edge.

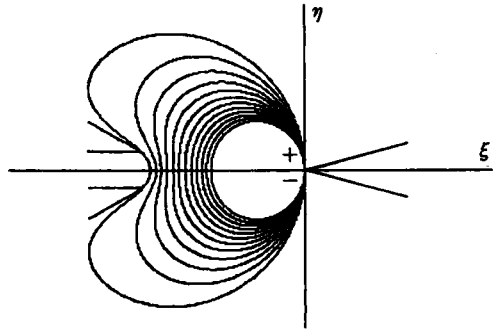

FIGURE 2. Approximate distortion of the dipole-induced streamlines by the presence of the nozzle (computed after Powell 1961).

tions from the edge loading-induced upstream influence as well as those arising from the jet instability. Bechert (1983) and Bechert & Stahl (1984) assert, in an analogous study of a mixing layer subjected to external, piston-like forcing that the pressure and velocity fluctuations can be decomposed into fluctuations induced by forcing and into those of the instability wave. Experimental evidence for the simultaneous presence of the upstream-induced field and the jet instability wave will be given herein in the section on velocity measurements, where a simple superposition model will be presented.

The foregoing description of the physics of the upstream influence and of the initial perturbation in the most receptive region of the jet is true for any distribution of fluctuating singularities on the edge with opposite sign on the lower and upper surface of the edge. D. G. Crighton (1984, private communication) has carried out an analysis employing a vortex-sheet representation of the jet embodying distortion effects both in the vicinity of the nozzle exit and the downstream leading edge; he finds the source at the edge to be of the split-multipole type. Herein, we employ the dipole concept to provide a view as simplified as possible, since the basic principle of jet excitation by upstream influence remains the same.

In the case of forced oscillations of the leading edge, there will be additional pressure loading on the edge at the frequency of oscillation and, accordingly, the upstream influence will also include this component. For purposes of illustration, we can consider the simplest case of edge oscillations at a frequency f_e in a quiescent

fluid. Imposing the constraint of small amplitudes of oscillation and neglecting viscosity, the pressure fluctuations at the frequency f_e on the upper surface of the edge will be in phase with the upward displacement and on the lower surface, the pressure will be π out of phase. The induced potential-flow field can be modelled with a dipole distribution on the edge. Simplifying this distribution with a single, fluctuating dipole and furthermore neglecting presence of the nozzle, we can write for the potential:

$$\phi(t) = \mu \cos 2\pi f_e t \frac{-\eta}{\eta^2 + \xi^2}, \tag{1}$$

where μ is the dipole strength and ξ, η are coordinates according to figure 2.

The velocities v in the η-direction are

$$v = \frac{\partial \phi}{\partial \eta} = \mu \cos 2\pi f_e t \frac{\partial}{\partial \eta}\left(\frac{\eta'}{\xi^2 + \eta^2}\right). \tag{2}$$

Along the jet centreline,

$$[v]_{\eta=0} = -\mu \frac{1}{\xi^2} \cos 2\pi f_e t. \tag{3}$$

Thus, velocities induced on the negative ξ-axis (jet centreline) are π out of phase with the dipole fluctuations.

Applying the unsteady Bernoulli equation, the following expression emerges for the pressure fluctuations at f_e on the η-axis, which are in phase with the pressures on the (supposed) edge surface:

$$[p(t)]_{\eta=0} = -\rho \frac{\partial \phi}{\partial t} = \mu \rho \frac{1}{\eta} \sin 2\pi f_e t. \tag{4}$$

Comparing (3) and (4) we can conclude that there is a phase difference of $\frac{1}{2}\pi$ between the induced velocities on the negative ξ-axis and the loading upon the edge resulting from the pressure fluctuations on the edge surface (loading positive in positive η-direction). Experimental evidence for this important relationship will be given in §4 and in figure 11. The distortion of the flow field by the presence of the nozzle, of course, has no influence on the above-derived phase relation. Again, it must be emphasized that the simple dipole enables one to discuss the central features of upstream influence, especially phase relations, but does not describe the distorted flow field either in the leading-edge region or the vicinity of the nozzle.

In the actual case of the jet impinging upon the oscillating edge, shown in figure 3 with a photograph and a schematic, the phase relation between the pressure loading and the edge displacement is no longer fixed at a value of zero, as in the above case of edge oscillations in a quiescent fluid; it now depends upon the phase relation of the oncoming jet fluctuations relative to the edge displacement, and thereby the flow structure in the leading-edge region. Typically, for frequencies f_e of the externally driven edge oscillations, sufficiently separated from the frequency f_0^* of the 'natural' jet oscillations, we can expect an upstream influence that is composed of contributions at the excitation frequency f_e and the frequency f_0 of self-sustained jet oscillations, schematically depicted in figure 3; this dual-frequency upstream influence arises from the fact that the loading on the edge is dominated by these same two frequency components. The relative magnitudes of the contributions at these two components will vary depending on the structure of the incident jet and the local jet–edge interaction. In the region away from synchronization, one expects that, at sufficiently low amplitudes of edge displacement, the initial pertubations of the jet at the nozzle for the two frequency components coexist and be amplified in the jet shear-layer.

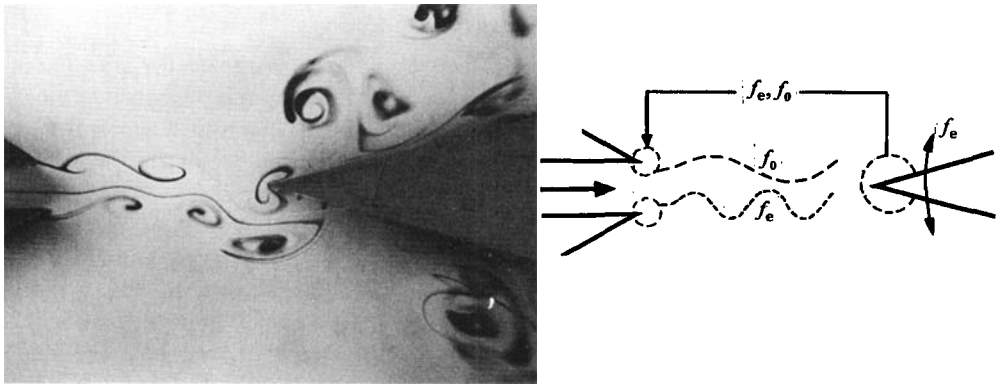

FIGURE 3. Jet impinging upon the oscillating edge ($f_e = 4f_0$).

Correspondingly, there will be modulations of the downstream-travelling waves and the associated vortex patterns. Indeed, as will be demonstrated subsequently, the periodicity T of the modulated flow patterns is given by the smallest common multiple of the two periods $T_e = 1/f_e$ and $T_0 = 1/f_0$.

On the other hand, if the forced oscillations of the edge are relatively close to the frequency f_0^* of the self-sustained oscillations, these two components will not develop independently along the jet. For f_e near or at f_0^*, the response of the jet will show typical characteristics of the response of a nonlinear, self-excited oscillator (with 'natural' frequency f_0^*) subjected to external forcing (at excitation frequency f_e); e.g. synchronization of the jet oscillations with the edge motion. External forcing of this oscillator in the form of a controlled displacement of the edge acts on the fluid at the system boundary, namely at the surface of the edge. The energy transferred to/from the flow field depends on the phase angle between the resultant force upon the edge surface and the displacement of the edge. This phase angle will undergo strong changes when the frequency f_e is near f_0^* as expected for any oscillator – linear or nonlinear – when it is excited near its natural frequency. A primary objective of this study is to relate this nonlinear response behaviour of the jet oscillations to the detailed flow structure of the jet.

In summary, there are a number of unexplored features of the edge loading and the flow structure arising from an unstable jet impinging on an oscillating leading edge. Among them are: the extent to which the excitation at the frequency f_e could influence the self-sustained oscillation at f_0 including the alteration of the value f_0 itself ($f_0 \neq f_0^*$); the possible existence of a range of synchronization and thereby a range of resonant response of the jet–edge interaction; the type of phase variation between the flow-induced loading and the edge displacement when the jet system passes through resonance; the possibility of attenuating the growth rate of the jet instability and reduction of the resultant fluctuating loading upon the edge by forced oscillations at an appropriate frequency; recovery of the self-sustained jet oscillations for forcing frequencies f_e away from synchronization; the existence of well-ordered modulation patterns in the flow depending on the frequency ratio f_e/f_0; and the types of vortex–vortex and vortex–leading edge interaction mechanisms associated with these modulation patterns.

2. Experimental system and instrumentation

The aims of this investigation were to characterize the response of the fluctuating pressures $p(t)$ on the surface of the edge, as well as of the velocity fluctuations $v(t)$ upstream of the edge, to forced oscillations of the edge. These measurements are interpreted in conjunction with flow visualization of the structure of the jet and its interaction with the edge.

Figure 4 shows an overview of the jet–edge arrangement. Details of the experimental system and the water channel are described by Lucas & Rockwell (1984). A planar, initially laminar jet issued from the nozzle exit. The ratio of the nozzle depth to width was 48, ensuring minimal sidewall effects. The velocity distribution at the nozzle exit showed a fully developed parabolic profile corresponding to a ratio of a mean velocity U to a maximum centreline velocity u_c of 2:3. The Reynolds number based on the nozzle width and the mean velocity U was kept constant in the experiments at $Re = 740$. This value of Reynolds number and the impingement length $L/B = 9$ were chosen to ensure self-sustained oscillations of the jet at a single predominant frequency, and to allow detailed flow visualization as well as adequate resolution of the pressure fluctuations on the surface of the edge. Furthermore, when the edge was oscillated at a frequency away from that of the self-sustained jet oscillation, the measured quantities showed for the above experimental conditions only two dominant spectral components, an important consideration for interrelating the flow visualization, the velocity fluctuations in the approaching jet, and the pressure fluctuations.

The frequency of the self-sustained jet oscillations and the occurrence of higher modes is sensitive to variations of the impingement length, as demonstrated by Powell (1961). In this context, the present investigation with fixed ratio L/B and Reynolds number should be considered as representative of the basic features of the jet–oscillating edge interaction.

As schematically depicted in figure 4, the leading edge was oscillated at a frequency f_e by means of a cam arrangement and a variable speed d.c.-motor. The drive and the leading edge were stiff enough to avoid any feedback of the fluid forces on the motion of the body. The lowest natural frequency of the mechanical system was at 45 Hz, well above the highest investigated frequency of about 7 Hz. The centre of rotation of the leading edge lay $19B$ downstream of the tip of the edge. Since the radius of the edge oscillation was at least 120 times larger than the maximum tip displacement, the motion of the tip was essentially perpendicular to the jet centreline. The edge displacement was measured with a linear potentiometer. The slight distortion of the sinusoidal displacement signal was mainly due to a second-harmonic component having an amplitude less than 1% of the fundamental. Thus, the displacement of the edge can be written as

$$\eta(t) = \eta_e \cos 2\pi f_e t, \tag{5}$$

where $\eta_e = A/B =$ relative displacement amplitude. Other excitation of the edge, besides sinusoidal, was not considered because of the nonlinearity in the response of the investigated jet oscillations.

Concerning the pressure measurements, the amplitudes of the predominant spectral components as well as the phase, relative to the edge displacement, were determined. Most of the pressure measurements were taken at pressure taps $1.26B$ downstream of the leading edge. Some preliminary measurements were performed at $0.38B$, showing qualitatively the same type of response as observed for the larger

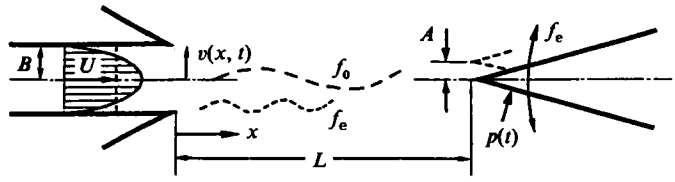

FIGURE 4. Jet–edge arrangement. $Re = 2UB/\nu = 740$; $B = 3.2 \times 10^{-3}$; $\eta_e = A/B$ = non-dimensional displacement amplitude; f_0^* = frequency of self-sustained jet oscillations (oscillating edge); f_e = excitation frequency.

distance. The selection of these positions was mainly based on measurements of Kaykayoglu & Rockwell (1986) who investigated the instantaneous pressure distributions on a stationary edge. Their investigation showed that the maximum pressure amplitude occurred for the investigated instability wavelength within a distance $1.5B$ from the leading edge; moreover, the phase variation of the pressure over a distance $1.5B$ downstream of the tip was less than $\frac{1}{5}\pi$, demonstrating that measurement of the fluctuating pressure at any location in the tip region is representative of the edge loading.

By making redundant measurements on the lower and upper surface it was possible to check symmetry conditions and to average the results. The maximum deviation of the pressure amplitudes on the lower and upper surface with respect to the averaged value was $\pm 5\%$, in general it lay between ± 1–2%. Furthermore, as demonstrated by Ziada & Rockwell (1983) for an analogous shear-layer configuration, and as experienced in preliminary stages of this study, free-surface effects could influence the pressure measurements as well as the overall characteristics of the flow oscillations. Such effects were avoided by covering the free surface of the test section with rigidly mounted styrofoam.

Calibration of the pressure transducer (Kulite Type XCS-190), including recalibration after the measurements, showed a repeatability of better than 1 %. From the scatter of the measured amplitudes an overall accuracy of better than $\pm 5\%$ can be estimated except for the spectral components of pressure having very small amplitudes, where the relative error might be higher; such small amplitudes occur in the case of quenched, self-sustained pressure fluctuations (figure 6*b*).

The response characteristics of the measuring system were examined by oscillating the edge in still water. These measurements (see figure 5) confirmed that there is no distortion in amplitude or phase within the investigated frequency range.

Velocity measurements were focused on the v-component along the centreline of the jet (see figure 4) from a position 1 mm downstream of the nozzle to a position immediately upstream of the leading edge. The measurements were performed with a backscatter laser-Doppler anemometer (LDA) (TSI; Argon-ion, 2 watts) having a beam expander to optimize the signal-to-noise ratio. The data rate was sufficiently high to allow use of the analog output of the counter of the LDA system.

All displacement, pressure and velocity signals were digitized and processed by a minicomputer (DEC-MINC). Aliasing was avoided by appropriate filtering. Power spectra and cross-spectra were evaluated, from which the amplitudes of the spectral components at f_0 and f_e were determined, as well as phase shifts between pressure and displacement or velocity and pressure.

For flow visualization, food colour was injected through thin glass capillaries into the boundary layer on the lower nozzle wall and along the centre streamline between the plates well upstream of the nozzle. Also, dye was introduced by gravity at the

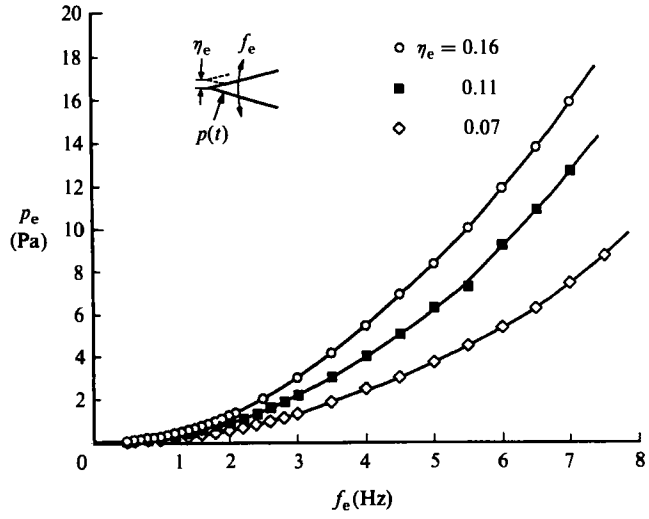

FIGURE 5. Pressure loading on the oscillating edge in the absence of jet flow for varying displacement amplitudes.

exterior of the upper lip of the nozzle where it was subsequently entrained into the upper shear layer of the jet. The time records of the flow patterns were recorded with a video camera (Instar by Video-Logic) at a rate of 120 frames/s.

The experimental data were acquired for one geometry ($L/B = 9$) and one Reynolds number ($Re = 740$). The varied parameters were the amplitude of oscillation $\eta_e = A/B$ and the excitation frequency f_e, which was the major parameter for characterizing the response functions of the sinusoidal oscillation of the tip of the leading edge. The time records of measured pressure fluctuations on the edge surface were analysed in the frequency domain, as well as velocity signals along the jet centreline.

The frequency f_0^* of the self-sustained jet oscillations in the absence of edge oscillations is used for normalization of frequencies; however, for discussion of flow visualization, the ratio f_e/f_0 also is employed. Although f_0 is a dependent variable, the ratio f_e/f_0 is the physically meaningful parameter that allows interpretation of modulations of the flow structure. Strouhal numbers, e.g. $S_e = Bf_e/U$, are not introduced explicitly because frequency ratios are of primary interest in this experiment with external excitation; moreover we note that $f_e/f_0^* = S_e/S_0^*$.

3. Pressure loading at the edge

Controlled sinusoidal displacement of the edge at amplitude η_e and frequency f_e, as defined by (5), allowed detailed examination of the response of the jet oscillation to external excitation. Most experiments were performed at constant η_e while varying f_e since the excitation frequency is the crucial parameter in determining the character of the shear-layer instabilities in the jet as well as the phase shift between the jet oscillations and the edge motion.

In general, the time records of the measured pressure signals showed a beating wave form, where the beat frequency corresponded to the difference between f_e and f_0. Spectral analysis of the signals showed the predominance of two frequency components at f_e and f_0, while amplitudes of higher harmonics, subharmonics and components at the sum/difference frequencies of f_e and f_0 were small. Measured

amplitudes of the second harmonic of f_0, which was the largest neglected term, was, at most, 20 % of the fundamental; the second harmonic of f_e was at maximum 5 % of the fundamental. Also, since no measurable frequency modulations were detected for the two components, the pressure fluctuations can be approximated by

$$p(t) = p_0 \cos 2\pi f_0 t + p_e \cos (2\pi f_e t + \phi), \tag{6}$$

where p_0 and p_0 are the amplitudes of the pressure fluctuations at f_0 and f_e. Pressures are generally non-dimensionalized with $\frac{1}{2}\rho U^2$, as shown in the subsequent graphs. However, in order not to complicate the presentation of equations, the ratio $p/(\frac{1}{2}\rho U^2)$ has not been introduced in equations.

The phase angle ϕ is defined as the phase shift between the pressure fluctuation at f_e on the lower edge surface and the displacement η_e defined by (5); ϕ was determined by the cross-spectrum between the pressure and the displacement signals.

Since the phase angle ϕ characterizes the phase shift between the local loading on the leading-edge region and the displacement, it provides an indication whether there is energy transfer from the flow to the oscillating edge or vice versa. If one defines the sign of the localized loading with respect to the pressure fluctuations on the lower surface of the edge then there is energy transfer from the fluid to the body for $0 < \phi < \pi$ and $2\pi < \phi < 3\pi$, whereas the converse occurs for $-\pi < \phi < 0$ and $\pi < \phi < 2\pi$.

All constants defining the pressure fluctuation $p(t)$ in (6), that is p_0, p_e, ϕ, and also the frequency f_0 of the self-sustained component, are functions of the forcing frequency f_e and of the amplitude of the tip displacement η_e.

In the following, we first assess pressure fluctuations induced by non-circulatory or 'added-mass' effects, associated with acceleration of the fluid surrounding the edge, by considering the oscillating edge in quiescent fluid. We then proceed to characterization of the pressures induced by the interaction of the jet with the oscillating edge.

3.1. *Pressure loading in the absence of jet flow*

The flow field and the pressure on the edge surface induced by oscillations of the edge in still water are essentially inviscid phenomena for the small amplitudes and frequencies of this study. From unsteady potential-flow theory we can show that the amplitude of the surface pressure at the excitation frequency f_e is proportional to the amplitude of the displacement η_e and the square of the frequency f_e:

$$p_e = k\rho\eta_e f_e^2, \tag{7}$$

where k is a geometry-dependent constant having the dimension of area. This relation, of course, is equivalent to the fact that the resultant force on the edge is proportional to edge acceleration.

Figure 5 shows experimental data acquired for edge oscillations in the absence of flow through the jet nozzle. For all three amplitudes of oscillation, $\eta_e = 0.07$, 0.11, 0.16, the amplitudes of the pressure fluctuations increase as the frequency squared in accord with (7). Furthermore, for constant frequency f_e, the pressure amplitude increases linearly with the displacement amplitude η_e. From these measurements, the constant k of (7) was determined to have the value $k = 2.1$ m^2 for the pressure tap located $1.26B$ downstream of the leading edge.

The corresponding phase shift between the pressure and displacement was negligible. An observed small, negative phase shift, due to minor viscous effects, reached a value of -0.15 rad at the largest amplitude of oscillation.

As noted previously, amplitudes of pressure fluctuations, as in figure 5, were averaged from measurements on the lower and the upper surfaces, allowing minimization of measurement inaccuracies. From additional experiments, involving oscillations of the edge with rigidly covered pressure taps, we could determine contamination of measured and averaged pressures of less than $\pm 2\%$ by signals induced through transducer vibration, edge deformation, or acceleration effects of the enclosed water mass between the transducer membrane and the pressure tap.

3.2. *Pressure loading on the stationary edge in the presence of the jet*

In the absence of edge oscillations, but in the presence of jet flow, self-sustained oscillations of the jet give rise to pressure fluctuations of the form:

$$p(t) = p_0 \cos 2\pi f_0^* t, \tag{8}$$

which is a special case of (6), where $p_e = 0$ and $f_0 \rightarrow f_0^*$. The measurements of amplitude p_0 for the stationary case are included in figures 6(*b*) and 7(*b*). Henceforth, we distinguish between f_0^* and f_0, representing respectively the self-excited oscillation frequency in the absence of, and in the presence of, external excitation; in general, f_0 differs from f_0^* owing to alteration of the jet structure by excitation. For the Reynolds number and geometry investigated here, we measured $f_0^* = 1.50$ Hz. This frequency remained constant for steady flow conditions once an equilibrium water temperature throughout the channel was achieved. Frequency modulations were less than $\pm 0.5\%$. The frequency $f_0^* = 1.50$ Hz corresponds to a Strouhal number $S_0^* = Bf_0^*/U = 0.041$, a value close to those found by other authors for comparable geometry and Reynolds number.

3.3. *Pressure loading on the oscillating edge in the presence of the jet*

In the case of edge oscillations we expect, in the general case, two frequency components to be present (as shown in (6)). We first address the manner in which the parameters p_0, p_e, f_0 and ϕ vary as a function of the dimensionless excitation frequency f_e/f_0^*. In particular, attention is focused on resonance characteristics of the oscillating jet system including synchronization of the self-sustained jet oscillations with the external excitation; and recovery of the inherent jet instabilities above synchronization.

Resonant response of the pressure fluctuations at the excitation frequency

Intuitively, we expect a resonant response when the edge is oscillated at a frequency identical with that of the self-sustained jet oscillations. Indeed, figure 6(*a*) shows a distinct resonance peak in the distribution of the pressure component p_e for excitation frequencies near f_0^*, i.e. $f_e/f_0^* \approx 1$. The pressure p_e decreases for low excitation frequencies and reaches zero for $f_e = 0$. At $f_e/f_0^* \approx 2.5$ the graph shows a second, broader maximum. Owing to the variation of f_0/f_0^* with f_e/f_0^* (discussed subsequently), this second maximum physically corresponds to three periods of the externally excited oscillation at f_e within one period of the self-sustained oscillation at f_0.

Furthermore, at sufficiently high ratios of f_e/f_0^* the non-circulatory or 'added mass' contribution to the pressure fluctuation p_e at frequency f_e dominates, evidenced by the fact that the data of figure 6(*a*) approach the curve corresponding to no-jet flow; it is designated by the dashed line, which represents the data of figure 5. In essence, this means that the local interaction of the forced jet oscillations with the leading edge is not significant in determining the surface pressure amplitude at frequency f_e for sufficiently high ratios f_e/f_0^*.

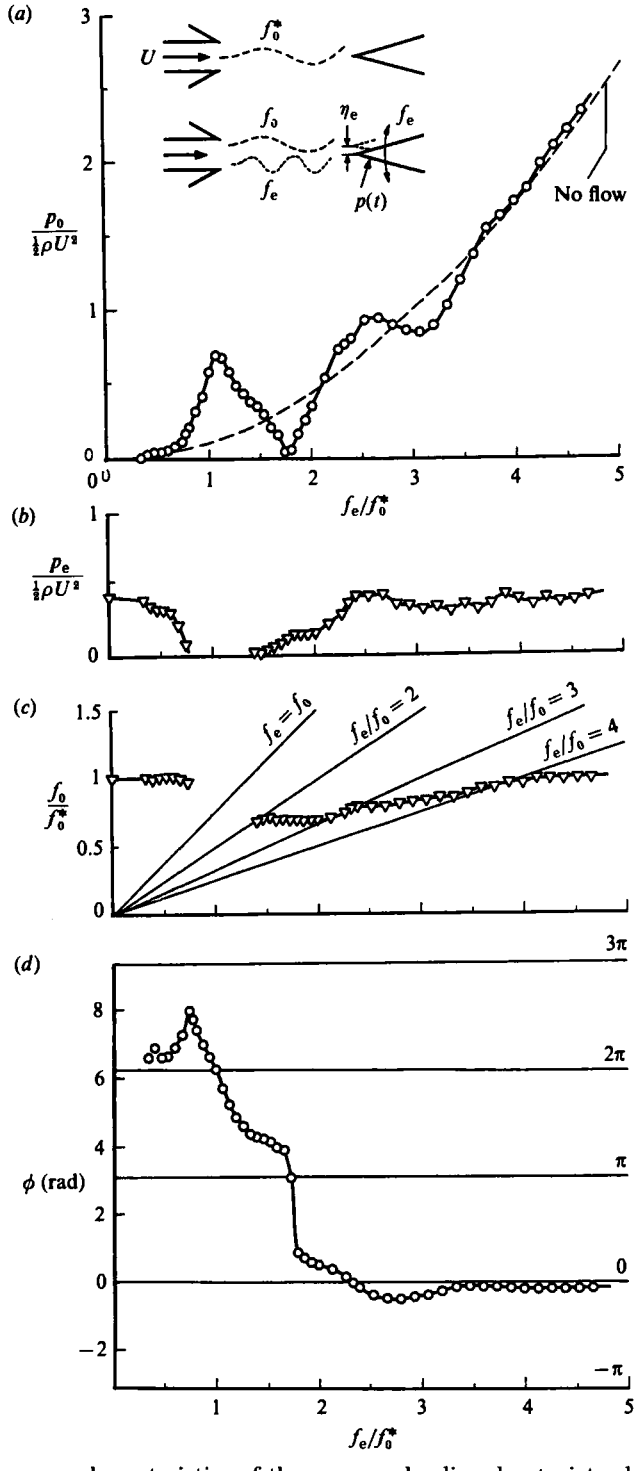

FIGURE 6. Response characteristics of the pressure loading due to jet–edge interaction showing: (*a*) externally excited pressure component p_e; (*b*) self-excited pressure component p_0; (*c*) frequency f_0 of the self-sustained jet oscillation; and (*d*) phase ϕ between the pressure fluctuations at f_e and the displacement $\eta(t)$. Amplitude of edge displacement $\eta_e = 0.16$; $Re = 740$.

Quenching and recovery of self-sustained pressure fluctuations

In general, the self-excited pressure component p_0 will be present simultaneously with the externally induced component p_e. However, as demonstrated in figure 6(*b*), as the frequency ratio f_e/f_0^* approaches 1, either from the higher or lower side, p_0 experiences rapid attenuation. Comparing with figure 6(*a*) in this same range, p_e undergoes a rapid increase in amplitude corresponding to onset of resonance. This range of dimensionless excitation frequency f_e/f_0^* for which the edge oscillation synchronizes with the jet oscillation at the frequency f_e and, therefore, only the component p_e can be determined, is termed the 'synchronization range'. In general, such synchronization can be obtained by either phaselocking the self-excited oscillation at f_0 to that of the forced oscillation at f_e, or by simply attenuating the self-excited component down to zero amplitude. This second means of achieving synchronization is called 'quenching' according to Dewan (1972) and is further discussed for different flow oscillators by Staubli (1985). The plot of the data in figure 6(*b*) indicates that, for the jet oscillations under consideration here, synchronization is achieved by quenching because of the strong attenuation and eventual suppression of the pressure amplitude p_0. This quenching of the self-sustained jet oscillation occurs at frequency ratios f_0/f_0^* considerably lower or higher than $f_0/f_e = 1$, as shown in figure 6(*c*).

Figure 6(*b*) further shows that for sufficiently high excitation frequency, $f_e/f_0^* > 2.5$, there is recovery of the amplitude of the self-excited component p_0 to that of the stationary edge ($f_e = 0$). This recovery is particularly remarkable in view of the fact that the externally imposed pressure fluctuations p_e at these high excitation frequencies have substantially larger amplitudes than those of the p_0 component. The physical mechanisms by which this recovery occurs, as well as the lack of influence on the self-sustained jet oscillations at very low excitation frequencies, are addressed subsequently in the section on flow visualization.

Alteration of self-excited frequency in the presence of the oscillating edge

In general, the self-excited oscillation frequency f_0 of the jet in the presence of edge oscillation deviates from the self-excited frequency f_0^* in the absence of external excitation. Figure 6(*c*) shows that for sufficiently low frequency ratios, $f_e/f_0^* < 0.7$, the frequency f_0 of the pressure component p_0 is relatively uninfluenced by the excitation. The largest influence occurs on the right-hand side of the synchronization range where the self-excited frequency deviates up to a maximum of 30 % from the frequency f_0^*. The ratio f_0/f_0^* is always lower than unity and recovers to a value of one as the excitation frequency increases. In certain ranges the self-sustained jet oscillation adjusts itself such that integer frequency ratios f_0/f_e are maintained, that is $f_0/f_e = 1/3$ or $1/4$. In other words, over certain ranges of the excitation frequency, the frequency ratio 'locks-on' to one of the f_0/f_e characteristics. These ranges correspond to local maxima in the pressures p_0 and/or p_e shown in figure 6(*a*,*b*). The associated structure of the jet will be described subsequently.

It is important to emphasize here that, near synchronization, the data do not approach the line $f_0 = f_e$ in figure 6(*c*). This means that not only is the self-excited component at f_0 attenuated at the onset of synchronization (figure 6*b*), but also there is no coalescence of the self-excited frequency f_0 and the excitation frequency f_e. This observation allows us to more precisely define the type of quenching as 'asynchronous quenching' (Dewan 1972).

Phase shift of pressure fluctuations relative to edge displacement

As the excitation frequency changes, there is a phase shift between the locally induced loading at f_e relative to the edge displacement η_e (see (6)). Figure 6(*d*) displays the phase ϕ of the pressure component p_e as a function of f_e/f_0^*. There is a strong gradient of this phase distribution as the excitation passes through the synchronization range. Such gradients are typical of linear or nonlinear systems undergoing resonance. On the other hand, for $f_e/f_0^* > 3.5$, the phase remains at a value near zero owing to dominance of the non-circulatory (added-mass) effects. The sharp drop in the phase of the order of π at a frequency ratio $f_e/f_0^* = 1.7$, i.e. at ratio $f_e/f_0 = 2.5$, is accompanied by a drop in amplitude of the pressure component p_e (figure 6*a*). In view of the fact that there is a phase jump, but nearly zero amplitude, one might call this region one of 'pseudoresonance'.

Effect of displacement amplitude on the response characteristics

The response of the jet to forced oscillations of the edge was investigated for two additional amplitudes of oscillation, $\eta_e = 0.11$ and 0.07. These smaller amplitudes were chosen because for sufficiently small excitation levels the onset of synchronization changes from 'asynchronous quenching' to 'phaselocking', and the two frequency components coalesce to the excitation frequency as synchronization is approached. This change in character in the onset of synchronization is expected because there is a lower limit in the amplitude of excitation, below which the self-sustained oscillations can no longer be attenuated or quenched. Physically, phaselocking means a systematic phase advancement or retardation of the self-sustained jet oscillation such that the two frequencies f_e and f_0 coalesce and both components, the forced and the self-excited, contribute to the pressure fluctuations at the same frequency, i.e. f_e.

Figures 7(*a,b,c,d*) shows a comparison of response characteristics of the pressure at edge amplitudes $\eta_e = 0.07$, 0.11 and 0.16. Comparing the three cases of displacement amplitude, there are substantial differences in pressure amplitudes p_e only for high excitation frequencies, figure 7(*a*). These differences are explained by the linear dependency of the non-circulatory (added-mass) contribution to the pressure on changes in displacement amplitude (see figure 5). The resonant pressure amplitudes p_e within the synchronization range ($f_e/f_0^* \approx 1$) show only minor changes due to the reduced displacement amplitude.

The effect of reduction in excitation amplitude η_e on the self-excited component p_0 (figure 7*b*) is more pronounced, especially near synchronization. As expected, when η_e is reduced, the attenuation of p_0 at the onset of synchronization is reduced and the actual range of synchronization gets smaller. In fact, for $\eta_e = 0.07$, there is no indication of complete suppression of p_0. Concerning the frequency f_0 of the self-excited component, figure 7(*c*) shows that the measured data points approach more closely the line $f_0 = f_e$ at lower amplitudes of displacement. This coming together of the two frequencies near synchronization, along with the smaller attenuation of the self-excited pressure, suggests that the character of the onset of synchronization changes from asynchronous quenching to phaselocking at the smallest investigated displacement amplitude of the edge.

Figure 7(*d*) shows the phase angle ϕ between the pressure component p_e and the edge displacement η_e. This phase shows astonishingly small dependence on displacement amplitude even though the latter varies by more than a factor of two, thereby indicating only minor nonlinearities of the excited component p_e with changes in displacement amplitude η_e.

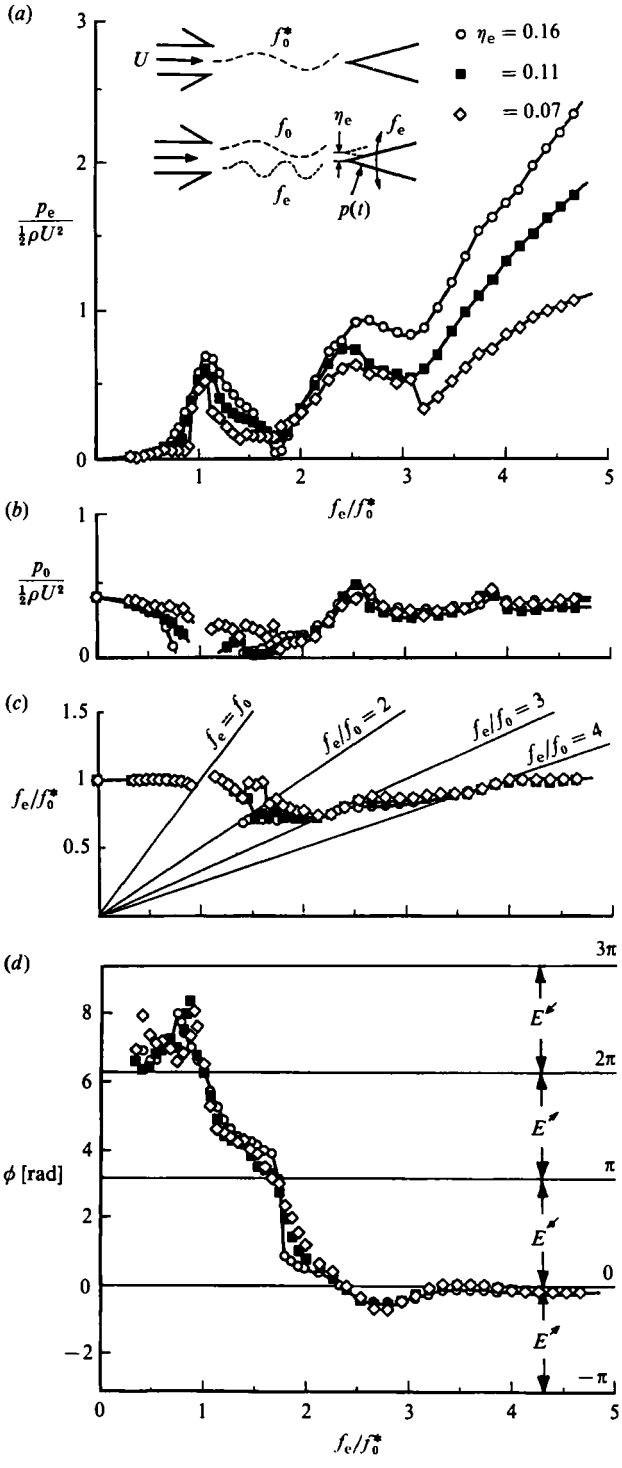

FIGURE 7. Response characteristics of the pressure loading due to jet–edge interaction for edge oscillations at various amplitudes showing: (*a*) externally excited pressure component p_e; (*b*) self-excited pressure component p_0; (*c*) frequency f_0 of the self-sustained jet oscillation; and (*d*) phase ϕ between the pressure fluctuations at f_e and the displacement $\eta(t)$. $E' + r$ = local energy transfer from the flow to the edge; $E' + r$ = energy transfer from the edge to the flow.

4. Phase characteristics of a jet approaching the oscillating edge

Spectral analysis of the velocity field of the modulated instability wave incident upon the edge showed dominance of the same two frequency components f_0 and f_e as in the pressure fluctuations. At a given location x along the centreline of the jet, one may represent the transverse velocity fluctuation v as

$$v(x,t') = v_0 \cos(\theta_0(x) - 2\pi f_0 t') + v_e \cos(\theta_e(x) - 2\pi f_e t'). \tag{9}$$

The phases $\theta_0(x)$ and $\theta_e(x)$ are the phase angles between the local velocity fluctuations and the reference pressure fluctuations p_0 and p_e on the edge at frequencies f_0 and f_e respectively. In (9) we have introduced the time t', which bears the following relation to the time associated with the displacement signal:

$$t' = \frac{\phi}{2\pi f_e} - t, \tag{10}$$

where ϕ is the phase shift between pressure component p_e and displacement η_e. The time t' is employed because the phase difference between the velocity and pressure fluctuations is physically more significant than that between velocity and displacement. The change of sign indicates waves travelling in the positive x-direction. In the experiment, the phases $\theta_0(x)$ and $\theta_e(x)$ were determined from cross-spectra between the velocity fluctuations at various x locations along the centreline and the pressure fluctuations at the edge.

Figure 8 shows the phase variation $\theta_0(x) - \theta_0(0)$ of the self-excited velocity component v_0 at frequency f_0 for different excitation frequencies f_e; $\theta_0(0)$ is the phase of the initial velocity fluctuation at the nozzle exit. The phase $\theta_0(x)$ does not grow linearly with x indicating wave non-homogeneity. For the stationary edge this observation has already been made by Shields (1967). Even though the jet is subjected to forced oscillations of substantial amplitude ($\eta_e = 0.16$), the phase distribution $\theta_0(x)$ of the self-sustained jet oscillations experiences insignificant alteration with f_e/f_0^*. This observation is somewhat surprising in view of the strong variations of frequency f_0 and pressure p_0 near synchronization (figure 6*b*,*c*) as well as of the substantial changes in the structure of the jet (figures 13–20). This relative invariance of $\theta_0(x)$ means also that the overall phase difference of the self-sustained jet oscillation remains essentially unaltered. However, since the self-excited frequency f_0 changes with f_e/f_0^* (see figure 6*c*) the local phase speed of the self-excited component, $c_{v_0}(x) = 2\pi f_0 / \mathrm{d}\theta_0(x)/\mathrm{d}x$, does undergo substantial modification with f_e/f_0^*, especially in the region just above synchronization.

Figure 9 shows the streamwise variation of the phase $\theta_e(x) - \theta_e(0)$ for the velocity component v_e at the excitation frequency f_e. At low frequency ratios f_e/f_0^*, we observe the same non-homogeneous character of the wave as was found for the self-excited component. For synchronization, $f_e/f_0^* = 1$, the measured phase curve is identical with the one measured for the stationary edge (figure 8). From mean slopes of the measured curves an averaged non-dimensional phase speed can be estimated:

$$\frac{c_{v_e}}{U} = \frac{2\pi f_e}{Uk} = \frac{2\pi f_e}{U(\mathrm{d}\theta_e/\mathrm{d}x)} = 0.36. \tag{11}$$

The wavenumber k, given by the mean slopes in figure 9, is therefore proportional to the excitation frequency. At higher excitation frequencies, several wavelengths ($6\pi = 3 \times 2\pi = 3$ wavelengths) of the forced jet oscillations can be observed over the impingement length and the phase distribution $\theta_e(x)$ takes on a stepwise distribution.

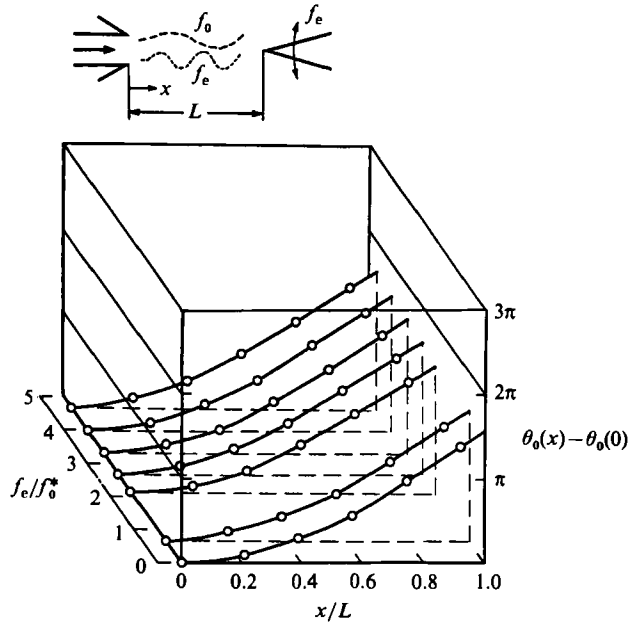

FIGURE 8. Phase variation of the self-excited velocity component v_0 along the jet centreline for different excitation frequencies f_e.

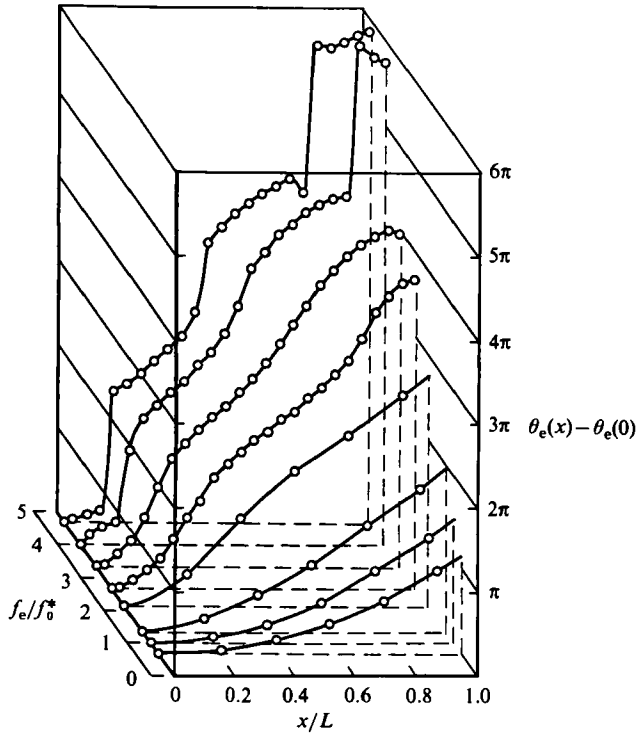

FIGURE 9. Phase variation of the externally excited velocity component v_e along the jet centreline for different excitation frequencies f_e.

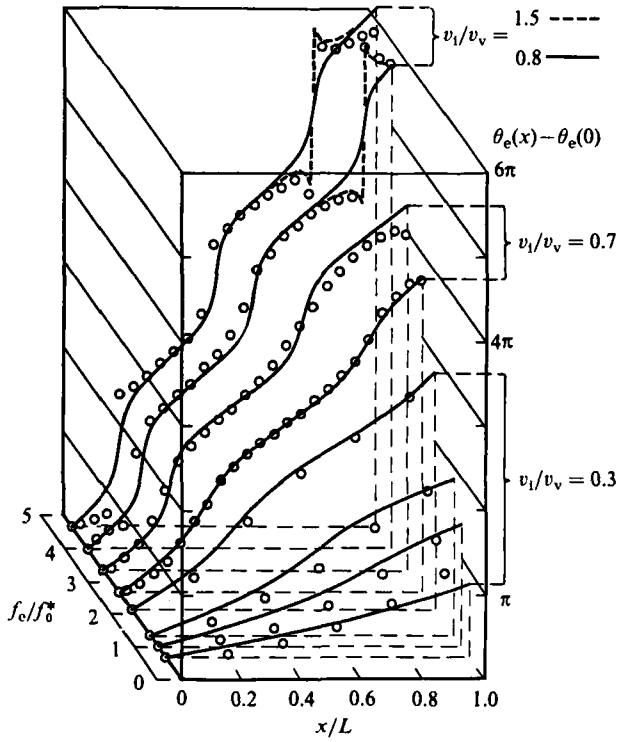

FIGURE 10. Comparison between phase variations computed with superpositions model (solid lines) and measured data points (circles).

This stepwise distortion suggests superposition of contributions from both the downstream-travelling instability wave, which we term a 'vorticity wave' (subscript v), and the irrotational fluctuation field induced by the pressure fluctuations on the edge surface, denoted as 'induced velocity' (subscript i) in the spirit of Powell's (1961) dipole-induced velocity fluctuations. Since the dimensionless frequencies $f_e L/a$ (a = speed of sound in water) are very low, the flow field is essentially incompressible and, therefore, there will be no streamwise phase variation of the induced velocity. Using the concept of superposition, we can represent the transverse velocity fluctuation at frequency f_e (second term of (9)) along the jet centreline as

$$v_e \cos(\theta_e(x)-2\pi f_e t') = \underset{\text{'induced velocity'}}{v_i \cos(\theta_{00}-2\pi f_e t')} + \underset{\text{'vorticity wave'}}{v_v \cos(\theta_{00}+\theta_v(x)-2\pi f_e t')}. \quad (12)$$

The phase angle θ_{00} is the phase of *induced* velocity relative to the pressure fluctuations on the edge.

To simplify the computations, while still retaining the basic concept of the superposition model, we further assume that: (*a*) the ratio v_i/v_v is constant over x; (*b*) the phase speed, $c_{v_e} = 2\pi f_e/k$, of the vorticity wave is constant over x and independent of f_e; and (*c*) $\theta_v(0) = \theta_{00}$. Putting (12) in explicit form for the phase $\theta_e(x)$, and employing the above assumptions, gives

$$\theta_e(x) = \theta_{00} + \operatorname{arccot}\frac{v_i/v_v + \cos(2\pi f_e x/c_{v_e})}{\sin(2\pi f_e x/c_{v_e})}. \quad (13)$$

The calculated distributions and the corresponding measured values of $\theta_e(x)-\theta_e(0)$ are displayed in figure 10. The relatively good agreement was attained

by empirically choosing the same dimensionless phase velocity of the vorticity wave, $c_{v_e}/U = 0.36$, for all excitation frequencies.

As noted in conjunction with figures 8 and 9, the wave character is non-homogeneous. The superposition-model explains this non-homogeneity well for high excitation frequencies and to a degree for low excitation frequencies; more accurate simulation requires accounting for the streamwise variation of phase speed, especially for frequency ratios $f_e/f_0^* < 1.5$. Moreover, it should be noted that increasing the ratio v_i/v_v for increasing f_e/f_0^* (see figure 10) provided a better fit of the computed curves to the measured data. This trend is because the pressure loading upon the edge induces a velocity amplitude v_i that varies, away from synchronization, as $v_i \sim f_e^2$, whereas the amplitude v_v of the vorticity wave is relatively invariant with f_e (for $f_e/f_0^* < 1.5$) because of the rapid nonlinear saturation of the amplifying disturbances. The ratio v_i/v_v dictates the severity of the sudden distortions in the phase distributions; ratios larger than unity (dashed lines) produce vertical jumps, agreeing well with the discontinuity in the measured data. Whereas the ratio v_i/v_v is responsible for the degree of distortion of the phase with x, the phase speed c_{v_e} determines the average slope of the phase variation.

Regarding the values of the phase angle at the nozzle exit, it was assumed that the velocity fluctuations v_i at frequency f_e induced by the pressure loading and the velocity fluctuations v_v arising from the vorticity wave are in phase at the nozzle, that is $\theta_v(x) = \theta_{00}$ in (12). At $x = 0$, the phase $\theta_e(x)$ of the resultant velocity component at f_e in (12) is $\theta_e(0) = \theta_{00}$, as can be derived from (13). The fact that the predicted locations of the sudden changes in phase agree well with the experimental data substantiates this assumption, indicating that the measured local pressure is representative of the loading on the edge and of the source of upstream influence.

Encouraged by the success of the above phase assumption in our model for velocity fluctuations at the excitation frequency f_e in (12), we further assume that the same phase of θ_{00} exists for the self-sustained jet oscillations at frequency f_e; as a result one can rewrite (9), evaluated at the nozzle exit ($x = 0$), as

$$v(0,t') = v_0 \cos(\theta_{00} - 2\pi f_0 t') + v_e \cos(\theta_{00} - 2\pi f_e t'). \tag{14}$$

The initial phase θ_{00} at the nozzle exit can be verified by measurements of $\theta_e(0)$ and $\theta_0(0)$. The variation of the measured phases for both the self-excited and the forced velocities at the nozzle exit, as a function of excitation frequency, is given in figure 11. The phases $\theta_0(0)$ and $\theta_e(0)$ are remarkably invariant and group with some scatter around the value of $-\frac{1}{2}\pi$. The deviation is highest near synchronization where there is a large gradient in the phase distribution of the pressure p_e (figure 6*d*). In §1 we deduced, from potential-flow considerations, a phase of $\theta_{00} = -\frac{1}{2}\pi$ between the velocity induced at the nozzle by the upstream influence of the pressure loading at the leading edge, which is basically confirmed by the measurements shown in figure 11.

In conclusion, the foregoing phase relation at the nozzle exit shows that the mechanism of upstream influence can be explained by an induced velocity at the nozzle exit whose time derivative is proportional to the fluctuations of the loading upon the edge. For the sinusoidal components in which the time records were decomposed here, there is a phase shift of $-\frac{1}{2}\pi$ between the velocity fluctuation and the loading for each of the fluctuation components. The generalized formulation that the time derivative of the initial transverse velocities is proportional to the pressure loading upon the edge can be expected to be true also for other types of edge displacement than the sinusoidal oscillations considered in this study.

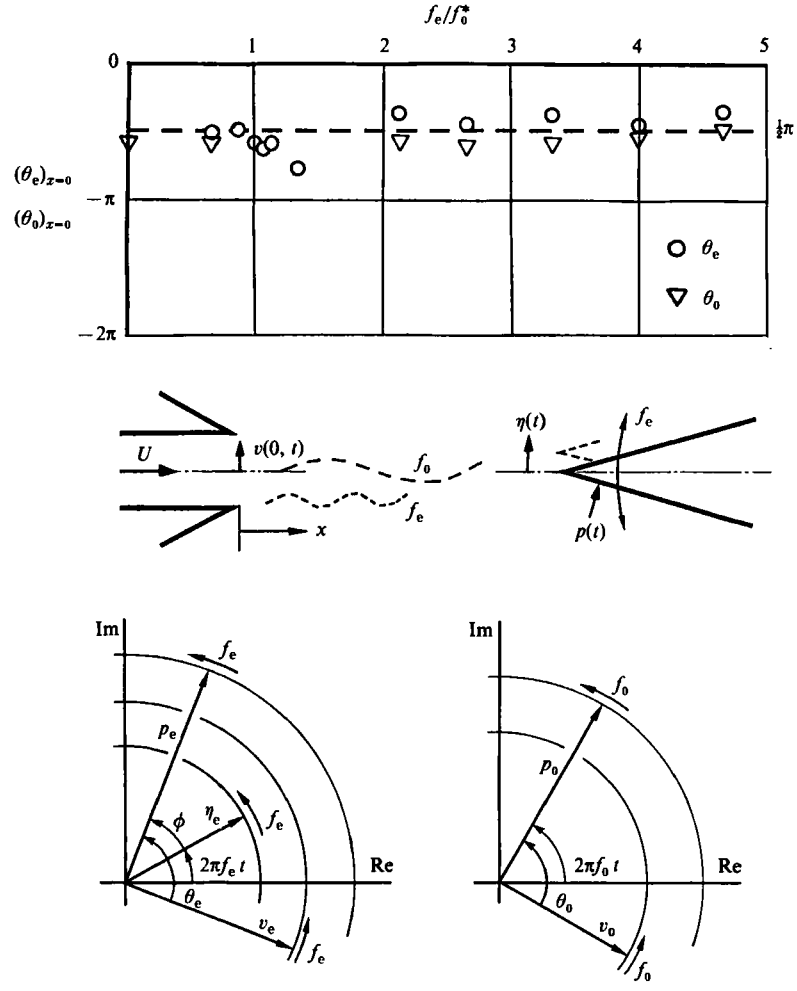

FIGURE 11. Phase relation between the transverse velocity fluctuations v_0 and v_e at the nozzle exit and the pressure fluctuation at the edge. $\eta_e = 0.16$, $Re = 740$.

5. Visualization of flow structure

The flow structure of the interaction of the jet with the oscillating leading edge was visualized by dye streaklines marking the jet undulations and the process of vortex formation at the self-excited frequency f_0, as well as at the excitation frequency f_e. The jet structure was visualized in the synchronization range, where the flow pattern repeats after each cycle of edge oscillation, as well as at frequencies below and above synchronization where there are modulations according to the occurrence of the two frequency components at f_0 and f_e.

The frequency ratios f_e/f_0^* selected for visualization are designated in figure 12 on plots of p_e, p_0 and $p_e \sin\phi$. Since ϕ is the phase angle between the pressure fluctuation p_e and the edge displacement $n(t)$, $p_e \sin\phi$ represents the pressure component that is in phase with the edge velocity. When $p_e \sin\phi$ is positive, there is a local transfer of energy from the edge to the fluid and when it is negative, there is a transfer of energy from the fluid to the edge. In selecting the frequency ratios f_e/f_0^* for visualization, several points were chosen within the synchronization range

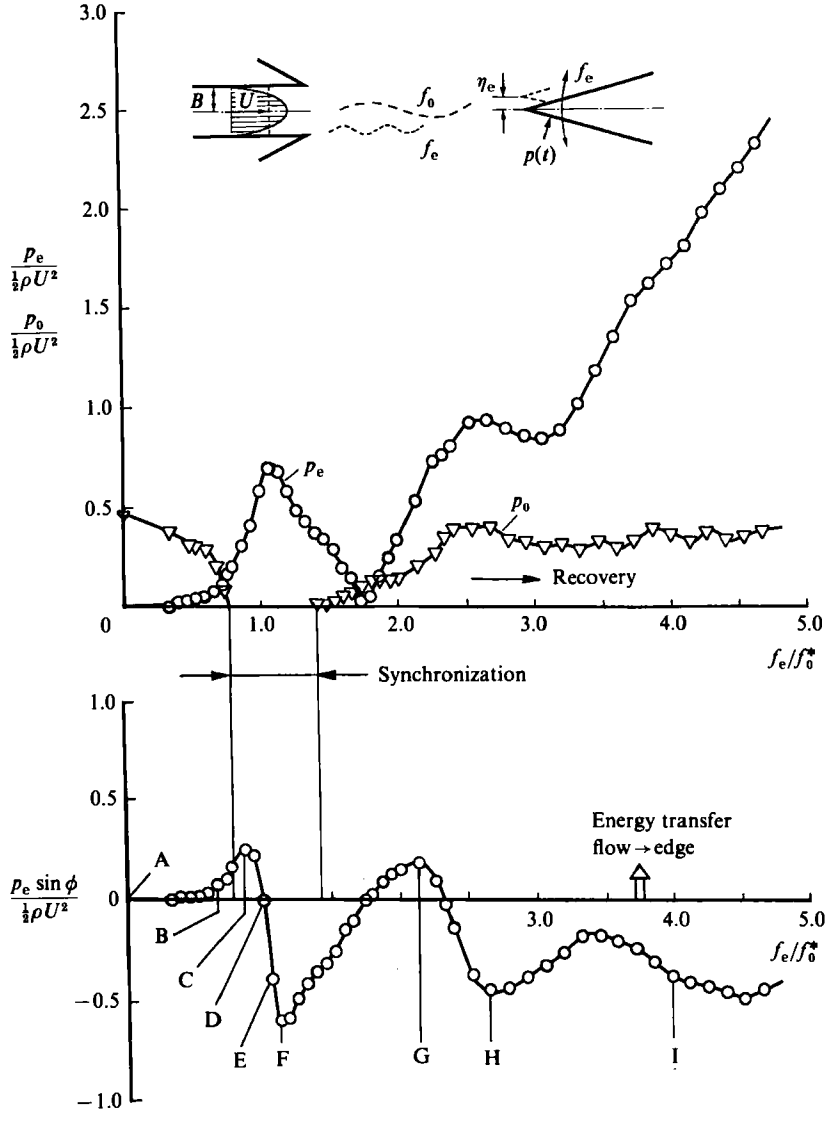

FIGURE 12. Overview of conditions selected for visualization (Cases A–I) in relation to the coexisting pressure amplitudes p_e and p_0 and the phase ϕ of the pressure p_e relative to the edge displacement $\eta(t)$.

(C, D, E, F). These points cover a range with strong changes in ϕ (see also figure 6*d*) and include the points with maximum positive and negative energy transfer (C and E). Further points were selected below (B) and well above synchronization (G, H and I). As a reference case, the self-sustained jet oscillations with the stationary edge (A) was chosen.

In general, it is possible to classify the jet structure into the following categories: self-sustained, 'natural' jet oscillations for the stationary edge; modulation of the jet structure below synchronization; jet oscillations synchronized with the edge oscillations; and modulation above synchronization. Within the synchronization range, visualization shows the possibility of attenuating the jet oscillation, corresponding to the case of maximum energy transfer from the fluid to the edge. More-

over, recovery of the large-scale structure to that of the stationary edge can occur for modulation of the flow structure above synchronization. In the following, we characterize in detail the jet structure corresponding to these various regimes.

5.1. *Regimes of flow structure of jet–oscillating-edge interaction*

In characterizing the possible flow regimes as a function of frequency ratio f_e/f_0^*, we employ the case of the stationary edge as a reference (figure 13). In the subsequent photo series, the time interval between photos corresponds to either one quarter of the externally excited period $T_e = 1/f_e$ or one quarter of the self-excited period $T_0 = 1/f_0$. All photo sequences showing the oscillating edge start with the edge at the maximum positive displacement. This phase reference for each photo sequence allows cross-comparison between the flow patterns at different excitation frequencies within the synchronization range.

For excitation below or above synchronization, there are modulations of the flow structure arising from coexistence of jet undulations at f_e and f_0; consequently both periods, T_e and T_0 must be considered for comparison.

Interaction of the jet with the stationary edge: self-sustained jet oscillations

The photographs of figure 13, corresponding to case A (figure 12), represent the interactions of the jet with the stationary edge, i.e. $f_e/f_0^* = 0$. Over the cycle of jet oscillation, there is a rapid growth of the inherent shear-layer instability of the jet leading to formation of a primary vortex; interaction of the jet with the leading edge gives rise to a secondary, counter-rotating vortex; and in turn, the primary and secondary vortices form a vortex pair. This counter-rotating vortex pair subsequently moves downstream and away from the surface of the edge. Concerning the corresponding pressure fluctuation at the surface of the edge, maximum positive pressure occurs on the lower surface of the tip, at approximately $t = 0$, again appearing after one period, i.e. $4/4\ T_0^*$. Simultaneously, there is at $t = 0$ a pressure minimum along the upper surface, associated with the onset of separation there (Kaykayoglu & Rockwell 1986).

Modulation of the jet structure at low excitation frequencies

The lower set of photos in figure 14, representing case B (figure 12), shows modulation of the jet oscillation due to coexistence of the two frequencies f_e and f_0; the frequency ratio is $f_e/f_0 = f_e/f_0^* = 2/3$. At $t = 0$ the edge is at maximum positive displacement and, correspondingly, for $2/4\ T_e$ at maximum negative displacement. The period of this modulated jet oscillation is $T = 2T_e = 3T_0$. The flow patterns are remarkably repetitive at this period T. If we trace the three periods of the self-sustained oscillation in this series of photographs, we can compare the following pictures with the stationary case of figure 13:

Case A		Case B	
$t = 0;\ 4/4\ T_0^*$	$\leftrightarrow$	$t = 0;\ 12/4\ T_0$	$(8/4\ T_e)$
$1/4\ T_0^*$	$\leftrightarrow$	$9/4\ T_0$	$(6/4\ T_e)$
$2/4\ T_0^*$	$\leftrightarrow$	$6/4\ T_0$	$(4/4\ T_e)$
$3/4\ T_0^*$	$\leftrightarrow$	$3/4\ T_0$	$(2/4\ T_e)$

This comparison of the self-sustained jet oscillation, with and without edge oscillation, indicates the changes in the flow patterns due to the edge motion; however, it is evident that the basic structure in case B is dominated by the self-sustained oscillation.

FIGURE 13. Self-sustained jet oscillations in presence of the stationary edge, corresponding to case A, $f_e/f_0^* = 0$.

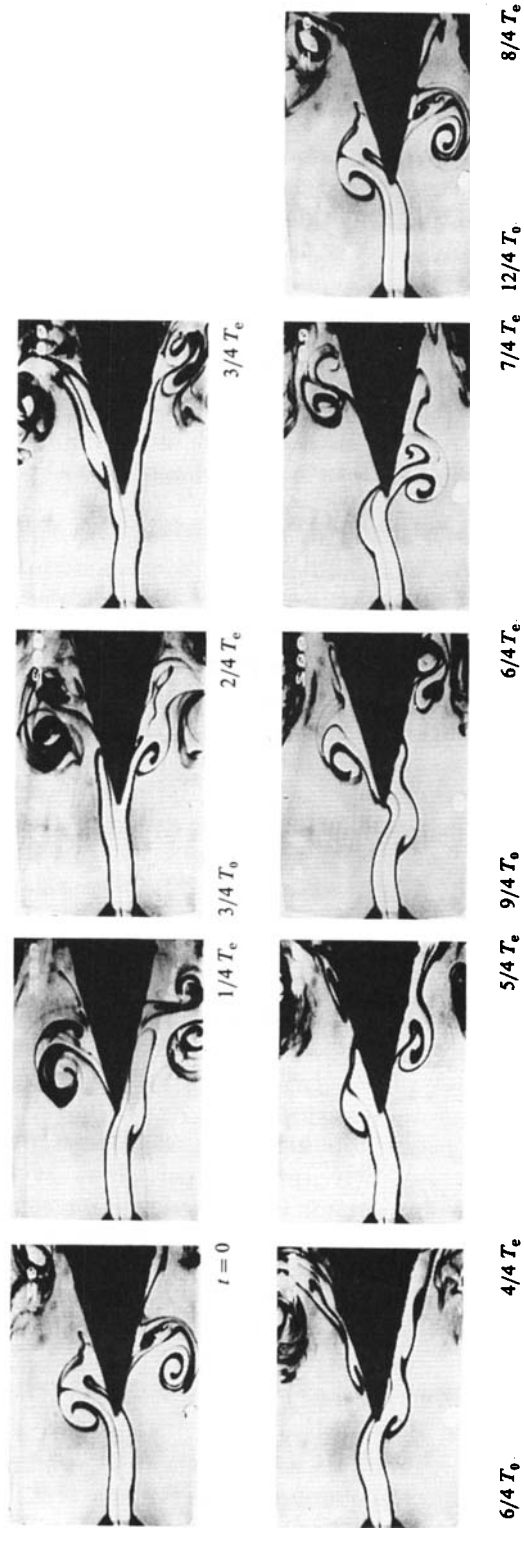

FIGURE 14. Modulation of the jet structure at low excitation frequency, corresponding to case B, $f_e/f_0^* = f_e/f_0 = 0.67$.

Synchronization

The photo sequences of figures 15 and 16, taken within the synchronization range, represent cases C, D, E and F (figure 12). Here, the edge oscillations control the jet oscillations and we expect repetitive flow structure after each cycle of edge oscillation. In figure 15, case C, with a frequency ratio $f_e/f_0 = 0.87$, represents the situation of marginal synchronization at the lower limit of the synchronization range. The photos show that the flow structure is indeed repeatable with the period T_e of the edge oscillation. Particularly interesting is the fact that for this excitation condition, the growth of the jet instability is actually retarded relative to case A of the stationary edge. Comparing respective photographs of cases A and C shows that roll-up of the primary vortices occurs further downstream for case C relative to case A. As shown in figure 12, case C represents the oscillation frequency where there is a maximum energy transfer from the flow to the surface of the edge. The energy extraction from the flow oscillation in this case actually retards the growth of the jet instability owing to an appropriate phase shift of the edge motion and the jet oscillation. Therefore, at this excitation condition, we can interpret the oscillating edge as an active damping element for the flow oscillation.

Figure 16 compares three cases, D, E and F, lying within the synchronization range. In general, the structure of the jet at these excitation frequencies is very similar to that of the stationary edge. Despite the onset of resonance of the pressure amplitude p_e over this range (figure 12), the basic jet structure undergoes insignificant alteration relative to the stationary edge (case A in figure 15). The phase ϕ between the pressure fluctuation p_e and the edge displacement η_e, as shown in figure 6(*d*), also undergoes dramatic changes since the cases D, E, F lie within the phase jump. That is, for the frequency ratios $f_e/f_0^* = 1$, 1.07 and 1.13, the respective phase angles are $\phi = 6.27$, 5.69 and 5.24; thus the phase difference between D and E is $\approx -\frac{1}{5}\pi$ and between D and F $\approx -\frac{1}{3}\pi$. Examining the photos of cases D, E and F at the same instant during the cycle, e.g. at $2/4T_e$ showing a vortex on the upper surface of the edge, it is evident that the locations of corresponding vortices move upstream with increasing excitation frequency, explaining the observed negative phase shift.

Modulation of jet structure at excitation frequencies above synchronization

Figure 17 shows a representative case of jet modulation at high excitation frequency, designated as case G ($f_e/f_0^* = 2.13$) in figure 12. Here the excitation frequency is three times the self-excited frequency, $f_e/f_0 = 3$. In other words, three cycles of externally imposed oscillations are required for one complete cycle of the modulated jet structure. The modulation period is $T = 3T_e = T_0$.

As expected, the forced vortices have shorter wavelength and mature more rapidly than at lower excitation frequencies, thereby allowing coalescence of vortices of the same sign, e.g. at $t = 9/4T_e$. The fact that the coalescence pattern of the forced vortices undergoes modulation indicates the presence of self-sustained jet oscillations. The streaklines of certain incident vortices are cut by the tip of the edge.

At still higher frequency of excitation, corresponding to case H in figure 18, the wavelength of the forced instabilities of the jet further decreases and the vortex formation appears closer to the nozzle exit. In this case, short time periodicity (i.e. small T) of the flow pattern does not occur since the ratio f_e/f_0^* cannot be described as a ratio of two small integer numbers, in contrast to the foregoing case. The theoretical frequency for repeating flow patterns would be $T = 10T_e = 3T_0$, which cannot be seen in figure 18 since only three periods of T_e are shown in the sequence

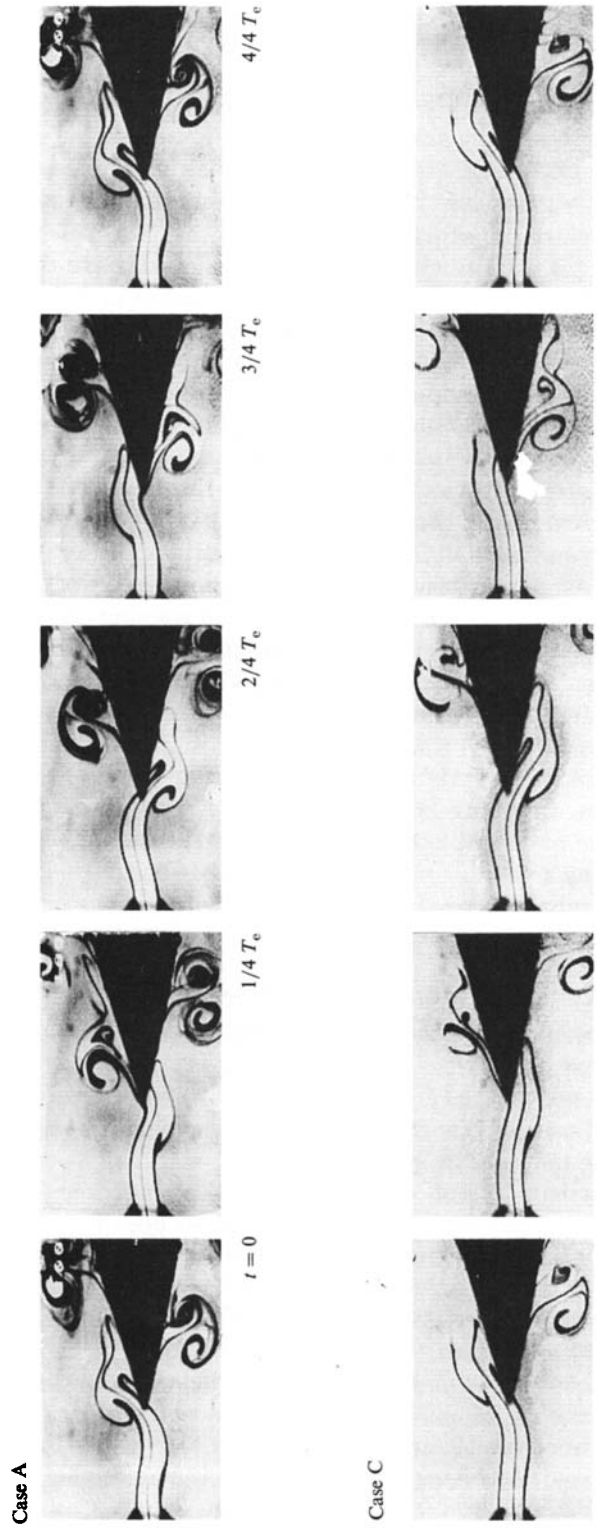

FIGURE 15. Comparison of the self-sustained jet oscillations ($f_e/f_0^* = 0$) and of synchronized jet oscillations corresponding to case C, $f_e/f_0^* = 0.87$. The excitation at frequency ratio $f_e/f_0^* = 0.87$ corresponds to a maximum in energy transfer from the flow to the edge and exhibits attenuation relative to the self-sustained oscillations of case A, $f_e/f_0^* = 0$.

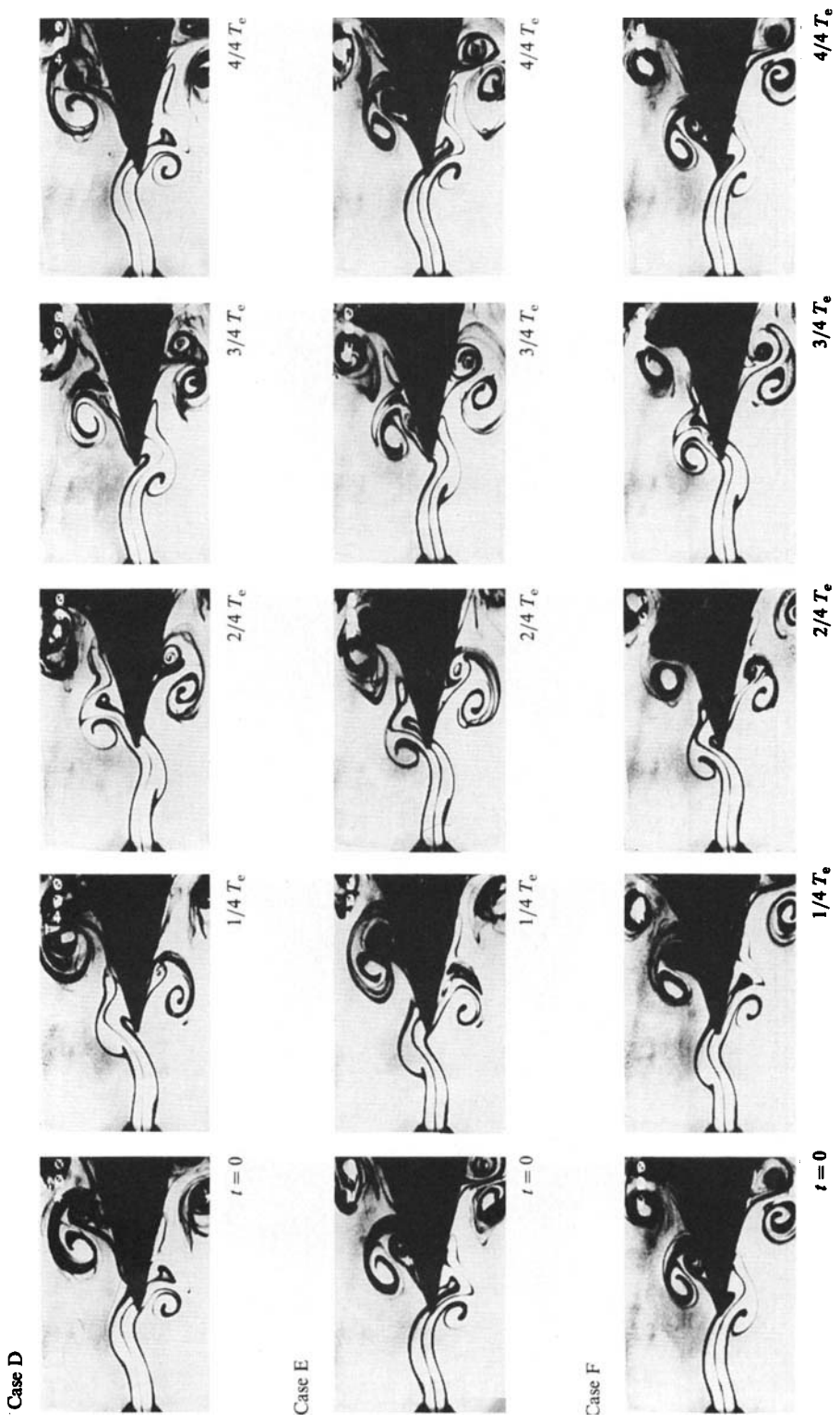

FIGURE 16. Comparison of jet oscillations, within the synchronization range, corresponding to the cases D, $f_e/f_0^* = 1.0$; E, $f_e/f_0^* = 1.07$; F, $f_e/f_0^* = 1.13$.

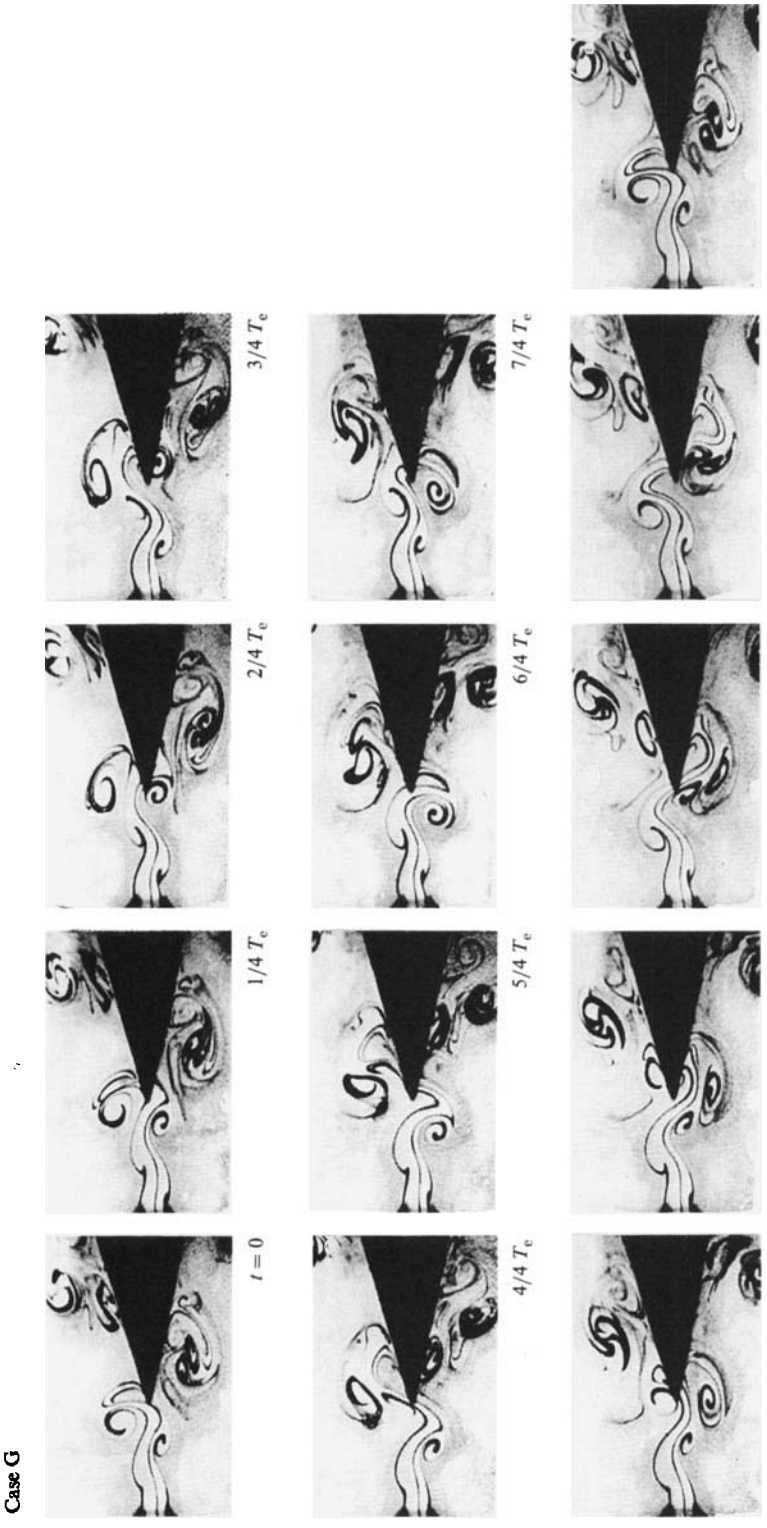

FIGURE 17. Modulation of the jet structure at an excitation frequency above synchronization, corresponding to case G, $f_e/f_0^* = 2.13$, $f_e/f_0 = 3$.

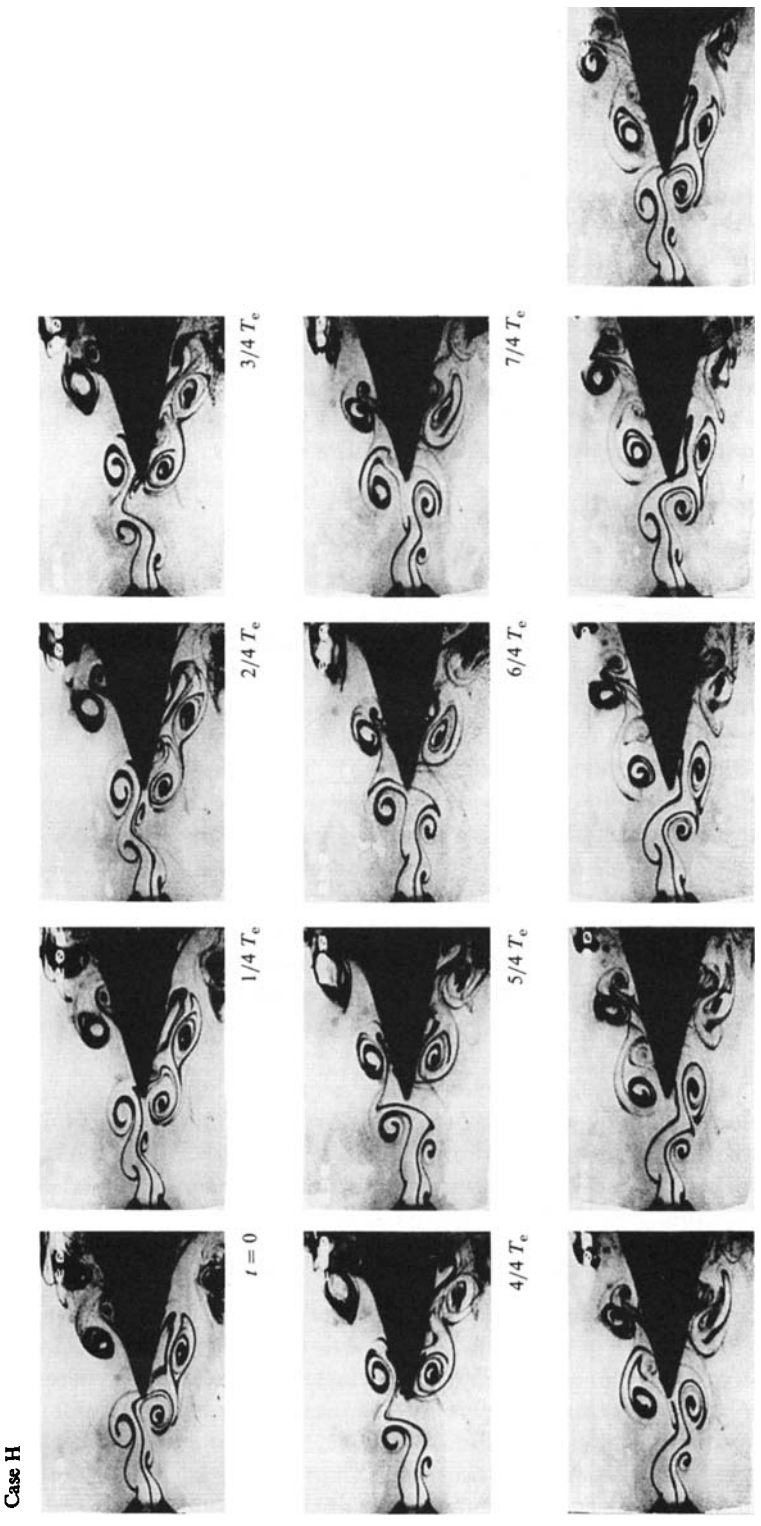

FIGURE 18. Modulation of the jet structure at an excitation frequency above synchronization, corresponding to case H, $f_e/f_0^* = 2.67$, $f_e/f_0 = 3.33$.

of photos. However, a distinct feature of the jet oscillation is that every third vortex on a given side of the jet passes to the opposite side of the edge, e.g. at $t = 3/4T_e$ or $10/4T_e$. For the region of the flow field upstream of the leading edge, this basic vortex pattern approximately exhibits a periodicity of $3T_e$, as is evident from the comparison of the photos at $t = 0$ and $12/4T_e$.

At the highest excitation frequency considered for visualization, corresponding to case I (figure 12), there are approximately 3 wavelengths of forced vortices within the impingement length, as shown in figure 19. In this case the frequency ratio is $f_e/f_0^* = 4 \approx f_e/f_0$ providing a period $T = 4T_e = T_0$ for repetition of the flow patterns. In this example, every fourth vortex from a given side of the jet passes to the opposite side of the leading edge. Particularly distinctive is the formation of a large-scale, counter-rotating vortex pair near the leading portion of the edge involving coalescence of three vortices of the same sign, which arrange into a pair with a vortex of opposite sense from the opposite shear layer. This vortex of opposite sense embodies the secondary vortex and obviously is fed with vorticity from the jet – leading-edge interaction on its motion downstream of the tip of the edge.

Recovery of self-sustained jet oscillations

According to figure 6(*b*,*c*), the frequency of the self-sustained oscillation, as well as the corresponding pressure amplitude p_0 are essentially uninfluenced by external excitation of the jet oscillation for excitation frequencies of $f_e/f_0^* \geqslant 4$. Flow visualization in this regime shows vortex formation in accord with coexistence of the two frequency components f_e and f_0. Closer examination of selected photographs in figure 19 shows that, at certain instants, the large-scale vortex patterns are quite similar to those of the self-sustained oscillations in figure 13, representing case A.

Figure 20 gives a direct comparison of the cases A ($f_e/f_0^* = 0$) and I ($f_e/f_0^* = 4$) over one cycle of the self-sustained jet oscillation. Comparing, for example, the large-scale vortex structure on the upper side of the edge, it is evident that the rapid vortex coalescence in case I leads to a vortex pair very similar to that in case A. Moreover other features, such as the deflection of the jet stem upstream of the leading edge, are quite similar at comparable instants during the cycle of the self-sustained jet oscillation. Consequently, we may conclude that coalescence of small-scale vortices leads to recovery of the large-scale, self-sustained jet oscillation.

Modulation frequency of the jet structure

In figures 13–20, we have addressed various features of the modulated jet structure for excitation frequencies below and above synchronization. On the basis of these observations, it is possible to put forth a simple relation which, in essence, states that the periodicity of the modulated flow pattern is determined by the smallest common multiple of the self-excited and the forced periods, $T_0 = 1/f_0$ and $T_e = 1/f_e$. In other words

$$T = nT_0 = mT_e = q/|f_0 - f_e|, \quad n, m, q = 1, 2, 3, 4 \ldots, \tag{15}$$

where n is the number of self-excited periods within T, m is the number of externally excited periods within T and $q = |n-m|$ is the number of beat periods within T.

Close examination of a number of periods T_e over the range of excitation conditions, in addition to the selected sequences shown here, shows for short T or small $|n-m|$, the foregoing relation is consistently valid. However, for long periods T, the flow patterns are not precisely repetitive indicating that there is minor frequency modulation of the frequency f_0. This frequency modulation is small, evidenced by the absence of observable broadening of peaks in the power spectra of the pressure measurements.

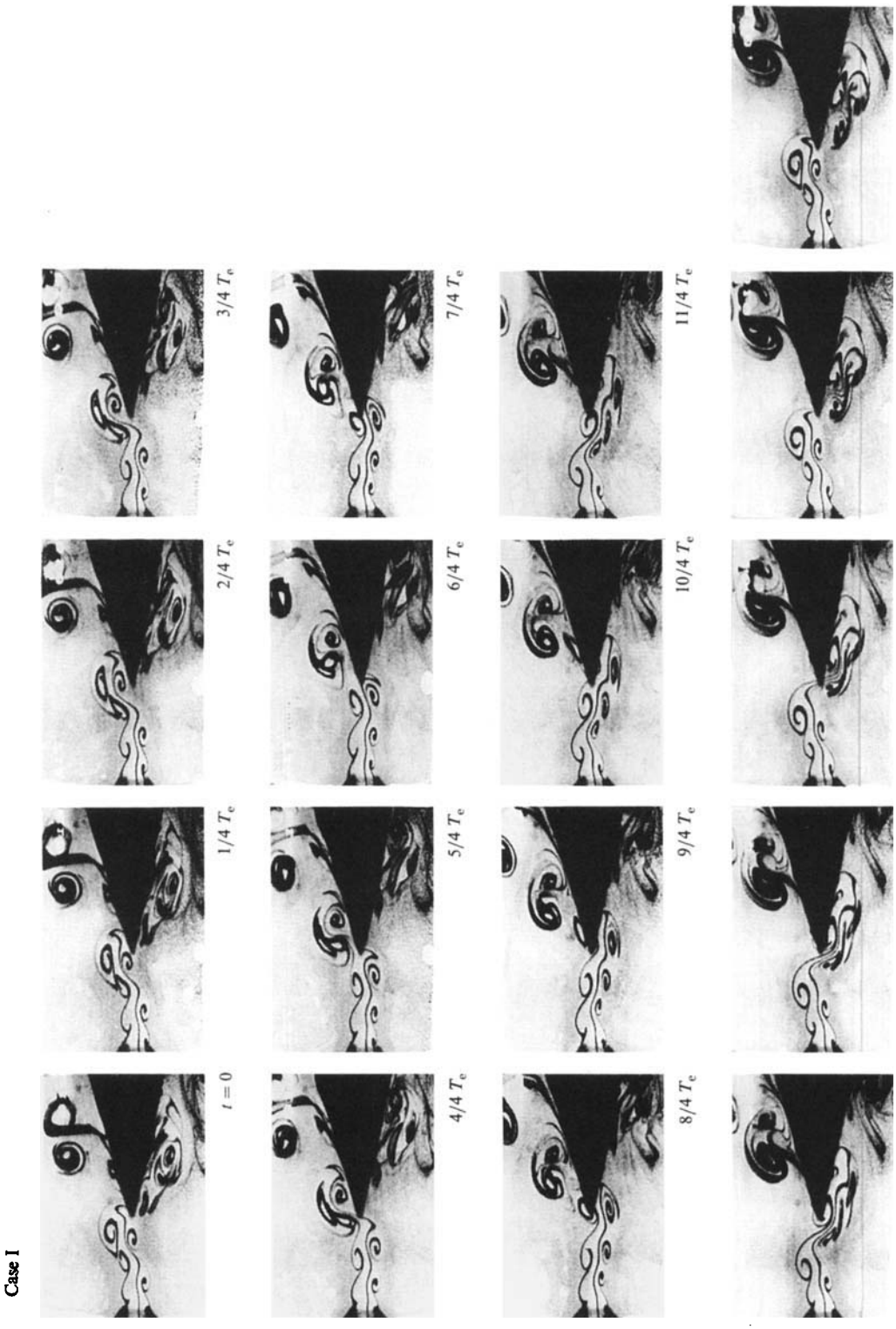

FIGURE 19. Modulation of the jet structure at an excitation frequency above synchronization, corresponding to case I, $f_e/f_0^* = 4.0$, $f_e/f_0 = 4.13$.

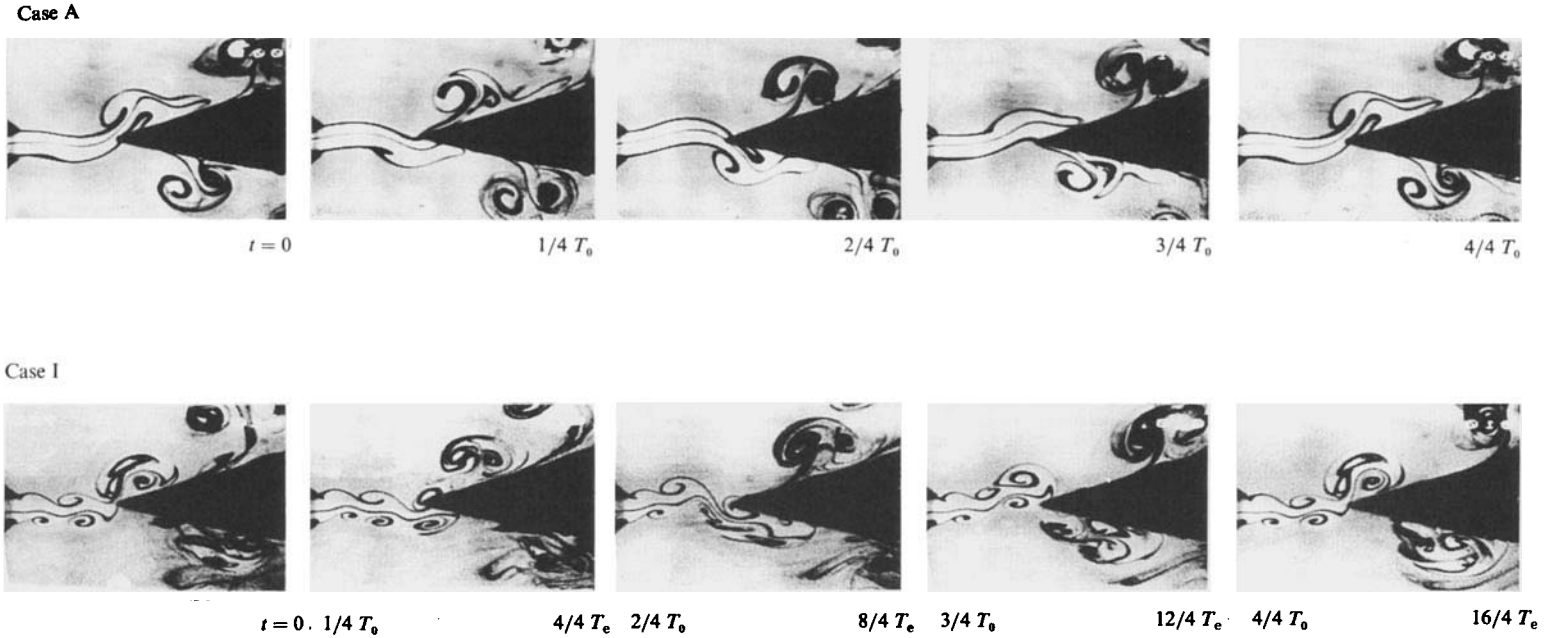

FIGURE 20. Comparison of one cycle of self-sustained jet oscillation for stationary edge (case A, $f_e/f_0^* = 0$) and for high frequency excitation (case I, $f_e/f_0^* = 4.0, f_e/f_0 = 4.13$) showing recovery of the large-scale, self-sustained vortex formation.

Summary of flow visualization

Characteristic of the low-frequency excitation is the fact that the typical wavelength of the forced jet oscillation becomes considerably larger than the impingement length L, e.g. for $f_e/f_0^* = 0.67$ there is only $\frac{1}{2}$ a wavelength within L, as can be seen in figure 9 from the fact that $\theta_e(L) - \theta_e(0) \approx \pi$. Further decrease of the excitation frequency will lead to even larger wavelength of the forced jet oscillations. At the same time there is, for the self-sustained oscillation, about $\frac{3}{4}$ of a wavelength within L. Since the excitation level, in terms of surface pressure fluctuations at the excitation frequency, also becomes very small at these low excitation frequencies, we observe a simple modulation of the self-sustained jet structure about a base structure. Figure 14 shows an example of the modulated structure at excitation frequencies below synchronization. Comparing the flow structure at low excitation frequency, case B, with the stationary case, case A, we see that the excitation causes momentary retardation of the self-sustained vortex formation (i.e. compare the small vortex structures at $3/4T_0$ of case B with those at $3/4T_0$ of case A, and at $6/4T_0$ of case B with those at $2/4T_0$ of case A) or it causes enhancement of the vortex formation (i.e. compare the large vortex structures at $6/4T_0$ of case B with those at $2/4T_0$ of case A).

Regarding the structure of the jet at high-frequency excitation, the photos of figures 17, 18 and 19 show substantial alteration of the jet structure relative to the stationary edge shown in figure 13. At higher frequency, the wavelength and the vortex scale become smaller and maturation of the vortex formation appears closer to the nozzle exit. For case G, the effect of the interaction is to hasten the coalescence of two adjacent vortices on the same side of the shear layer; meanwhile, the vortex of opposite sense from the opposite shear-layer is swept beneath the edge. For case H, corresponding to somewhat higher excitation frequency, this vortex coalescence is actually prevented by the fact that a vortex of opposite sense is swept to the same side of the edge; although it rapidly becomes undistinguishable, it preserves the spacing between two adjacent vortices. At still higher frequencies, case I, there is rapid coalescence of two vortices of like sense on the same side of the jet; the distinguishing feature of this interaction is that the vortex of opposite sense on the far side of the jet is swept to the upper side of the edge and grows in scale to arrange into a pair of counter-rotating vortices with the coalesced vortices. Concerning this coalescence, we note an interesting analogy with the phenomenon of collective coalescence as it has been assessed by Rockwell (1983) and Ho & Huang (1982) in free shear-layers of very long streamwise extent, whereby large-amplitude, low-frequency forcing causes several small-scale vortices to collect together. In figure 19, however, it is actually the self-excited jet oscillation at f_0 that drives the 'collective coalescence' of the small-scale vortices induced at f_e.

With respect to the energy transfer from the flow to the oscillating edge, we have seen that it reaches a maximum in the lower onset of synchronization. Flow visualization reveals that oscillation of the edge at the corresponding excitation frequency extracts not only energy from the flow oscillation but also leads to retarded growth of the jet instability, as shown in figure 15.

6. Conclusions

The flow structure arising from the interaction of a planar jet impinging upon an oscillating leading edge has been investigated by flow visualization, velocity measurements, and by pressure measurements. All three techniques reveal that the

self-sustained jet instability and the externally excited jet oscillation generally coexist simultaneously. Furthermore, there is a limited synchronization range where only one frequency component can be detected and where the flow pattern repeats exactly with the period of the edge oscillation. At the onset of synchronization the self-sustained jet oscillations are attenuated and eventually disappear at a frequency different from that of the excitation as can be seen from pressure and velocity measurement for the larger displacement amplitudes. For the smallest investigated amplitudes of edge displacement, the extent of the synchronization range becomes smaller and phaselocking is the mechanism leading to synchronization. Within the synchronization range resonance of the pressure component at the excitation frequency is observed. This resonance is accompanied by a strong gradient in the phase ϕ of the pressure fluctuations p_e relative to the edge displacement. The phase angle ϕ indicates the sign of the local energy transfer from the flow to the edge. In the case of maximum energy transfer from the flow to the edge, flow visualization shows that edge oscillation can actually dampen the jet oscillations.

Streamwise phase variations on the jet centreline indicate non-homogenous wave propagation and are, for the self-sustained jet oscillation, remarkably invariant with respect to the excitation frequency. The phase variation of the externally excited oscillation shows, for the higher excitation frequencies, stepwise phase distortion. This stepwise distribution in the phase of the transverse velocity component at the excitation frequency and, to a degree, also the non-homogeneous phase variation of the self-sustained component, are explained by superposition of contributions from: the velocity fluctuation of the downstream-travelling instability wave; and the upstream-induced velocity fluctuation originating in the pressure loading on the edge. At the nozzle exit, where the upstream influence dominates, we measure a $\frac{1}{2}\pi$ phase shift of the velocity fluctuations relative to the pressure fluctuations on the edge surface, agreeing with Powell's (1961) concept of upstream-induced velocities.

The stay of T. Staubli at Lehigh University was made possible by a grant from the Swiss National Science Foundation. Major project funding was provided by the Office of Naval Research, and supplemental funding was received from the National Science Foundation. Certain aspects of the flow visualization were supported by the Volkswagen Foundation.

REFERENCES

BECHERT, D. W. 1983 A model of the excitation of large scale fluctuations in a shear-layer. *AIAA Paper No.* 83-0724, *Presented at AIAA 8th Aeroacoustics Conf., April* 11–13, *Atlanta, Georgia.* 9pp.

BECHERT, D. W. & STAHL, B. 1984 Shear-layer excitation, experiment versus theory. *DFVLR. Rep.* DFVLR-FB 84-26. 84pp.

DEWAN, E. M. 1972 Harmonic entrainment of van der Pol oscillations: phaselocking and asynchrounous quenching. *IEEE Trans. Automatic Control.* AC-17, 655–663.

HO, C. M. & HUANG, L. S. 1982 Subharmonics and vortex merging in mixing layers. *J. Fluid Mech.* **119**, 443–473.

KAYKAYOGLU, R. & ROCKWELL, D. 1986 Unstable jet–edge interaction. Part I. Instantaneous pressure fields at single frequency. *J. Fluid Mech.* **169**, 125–149.

LUCAS, M. & ROCKWELL, D. 1984 Self-excited jet: upstream modulation and multiple frequencies. *J. Fluid Mech.* **147**, 333–352.

POWELL, A. 1961 On the edgetone. *J. Acoust. Soc. Am.* **33**, 395–409.

POWELL, A. 1962 Vortex action in edgetones. *J. Acoust. Soc. Am.* **34**, 163–166.

POWELL, A. 1965 Advances in aeroacoustics. *Rapports du 5^e Congrès International d'Acustique, Vol. II: Conférences Générales, Liège.*

ROCKWELL, D. 1983 Oscillations of impinging shear-layers. *AIAA J.* **21**, 645–664.

SHIELDS, W. L. 1967 An experimental investigation of the edgetone flow field. Dissertation, Department of Aeronautics and Astronautics, Stanford University, California, 67-17, 505. 73pp.

STAUBLI, T. 1985 Entrainment of self-sustained flow oscillations: phaselocking or asynchronous quenching? *ASME 10th Biennal Conf. on Mechanical Vibration and Noise, Fluid Structural Interaction, Cincinnati, Ohio.*

ZIADA, S. & ROCKWELL, D. 1983 Subharmonic oscillations of a mixing layer-wedge system associated with free surface effects. *J. Sound Vib.* **87**, 483–491.